Measurement-Induced Quantum Phase Transitions

Joseph Merritt

A dissertation
submitted in partial fulfillment of the
requirements for the degree of

Doctor of Philosophy

University of Washington

2023

Reading Committee:
Lukasz Fidkowski, Chair
Mark Rudner
Subhadeep Gupta

Program Authorized to Offer Degree:
Physics

University of Washington

Abstract

Measurement-Induced Quantum Phase Transitions

Joseph Merritt

Chair of the Supervisory Committee:
Associate Professor Lukasz Fidkowski
Department or Physics

There has been a recent increase in interest towards a nonequilibrium phenomenon called the measurement-induced quantum phase. These phases occur in "hybrid" systems where unitary evolution is interspersed with projective measurements. We look at two such systems. First we investigate a bosonic system of qudits. This is a one-dimensional chain with a d-dimensional local Hilbert space at each site. We forward a generalization of the stabilizer formalism to simulate hybrid dynamics on the system for certain prime numbers d and find evidence of both a measurement-induced entanglement transition and a measurement-induced purification transition. We find critical exponents $\nu \approx 1.3$ for all studied cases, consistent with known results for $d = 2$. We then investigate a fermionic system. Viewing the system as populated with Majorana fermions, we show a connection to a previously studied statistical mechanics model. We then generalize this model by leveraging the Gaussian state formalism. We simulate the hybrid dynamics of this generalized system under free fermion unitary evolution and measurement of local occupation number. We find evidence of a measurement-induced purification transition, and find the corresponding phase diagram. These models advance what is known about these classes of models and demonstrate the robustness of their corresponding measurement-induced quantum phases.

TABLE OF CONTENTS

Page

LIST OF FIGURES

Figure Number Page

ACKNOWLEDGMENTS

I have had an interesting time as a Ph.D. student, pandemic and all, and am happy to see how I have been influenced to grow as a person during this time. I would like to thank my advisor, Lukasz Fidkowski, for keeping me motivated during these years and providing direction for me. I would also like to thank the current and past members of my Supervisory Committee: Mark Rudner, Subhadeep Gupta, Silas Beane, Steffen Rohde, and Jayadev Athreya.

I would like to thank my fellow group members, Tyler Ellison, Ryan Lanzetta, and Sujeet Shukla for their support and collaboration. I would also like to thank my fellow graduate students for supporting me and giving me plenty of engaging (if not always productive) conversations: Kade Cicchella, Abhishek Rajput, John Goldak, and Dean Bretland.

I also want to give a big expression of gratitude to my brothers and sisters at the North Seattle Church of Christ for keeping me emotionally grounded, socially connected, and supporting me after I moved a thousand miles from home and had no connections in Seattle. Finally, I would like to thank my beautiful and brilliant wife Rachel, who gave me motivation, perspective, and support during my last year as a Ph.D. student.

Chapter 1

INTRODUCTION

For centuries, the study of phase transitions has been a rich subject in physics. During much of this history, investigations have focused on equilibrium phase transitions. In the past several decades, however, the physics of nonequilibrium quantum phase transitions has significantly advanced. Bolstered by advancing technologies in quantum preparation and manipulation, recent additions to this family of phenomena involve the study of "hybrid systems," or systems which evolve according to a process of unitary gates and projective measurements. These are the measurement-induced entanglement transition [1, 3] and the closely related measurement-induced purification transition [4, 5]. Advances in qubit control and measurement have allowed the recent experimental realization of these phases with current quantum devices [6, 7]. Theoretical advances include connections to quantum information and error correction [4, 8], topology in quantum systems [9, 10, 11], and conformal field theory [12, 13].

Simulations of quantum systems generally have to grapple with the many-body problem, as quantum state spaces are exponentially difficult to simulate on classical computers. We confront this challenge by developing two different numerical methods. In the first approach, we generalize an early model of a measurement-induced phase transition [1]: a bosonic system of qubits described by the stabilizer formalism. In this new setting, we advance an extension of the stabilizer formalism to describe qudits of prime order [14, 15] and demonstrate the existence of a measurement-induced quantum phase transition.

In the second approach we consider one-dimensional fermionic systems. These systems, as opposed to bosonic systems, have a natural free fermion limit. Despite the relative simplicity of free fermion systems, there is a wealth of nonequilibrium phenomena that have yet to be

fully described, including novel CFTs and an incomplete identification of universality classes. One advantage of this simplification is that free fermion systems can be efficiently represented in computations using the so-called Gaussian formalism. We exploit this feature to study a quantum-theoretic property of the system, called the *purity*, as it evolves under hybrid dynamics. The purity of a system can be seen in similar contexts as a measure of total quantum information in a system [4]. While the entanglement properties of monitored free fermions have been studied extensively, purity properties are not as well understood [5]. Using the Gaussian formalism, we uncover a purification transition between a mixed phase that protects quantum information and a critical "Goldstone" phase that exposes quantum information [16]. Furthermore, we demonstrate a connection to a previously known statistical mechanics model [2] and push the boundary of what is understood about this class of models. By using the Gaussian model to probe phases away from high symmetry points, we access phase transitions that were not previously available, an observation with relevance in a broader context.

In this introduction, we will provide the background of this novel class of nonequilibrium quantum phase transitions. We first review phase classifications from the full history of physics, focusing on what makes phases different from each other. We will introduce one of the first systems shown to theoretically exhibit a measurement-induced phase transition and use it to explain the concepts necessary to understand this class of transitions.

1.1 Equilibrium Phases

In this thesis, we rely on the differences between *equilibrium* and *nonequilibrium* phases. An equilibrium phase can be described by the properties of a system at thermodynamic equilibrium, such as global pressure, temperature, and chemical potential. By contrast, a nonequilibrium phase may have these quantities varying across the medium or have no way of defining these quantities. For instance, if such a system system reaches a steady state, there may still be fluxes of energy or mass through the system. These fluxes are not expected from a system in thermodynamic equilibrium.

We now give a short review of equilibrium phases, focusing on the qualitative differences that make phases distinct from one another.

1.1.1 Symmetry Breaking

From the 1940's to the 1970's, a number of physicists (most notably Landau and Ginzburg) established the paradigm of symmetry breaking phases. The core idea is one can distinguish a "disordered" phase from an "ordered" phase through symmetry. The ordered state has less symmetry than the disordered state i.e., in the ordered state there are fewer actions that will be a symmetry of the system than in the disordered state.

This is illustrated in the following two examples. Figures 1.1 and 1.2 show two systems where two distinct phases are differentiated using symmetry breaking. Fig. 1.1 demonstrates translational symmetry breaking. In the disordered phase, the system has full translational symmetry. More precisely, statistical mechanics describes the system as an ensemble of possible configurations, and this ensemble of states has complete, continuous translation symmetry. Intuitively, since the arrangement of atoms is random one can translate the system by any amount and the atoms will still have a random arrangement. In the ordered phase, however, this is not true. Since the system has a regular repeating crystal structure, not every translation is a symmetry of the system. The only translations which are symmetries for the ordered phase are the discrete translations in which every atom takes the previous location of another atom in the crystal. Therefore, the number of symmetries of the system has been reduced from a continuous symmetry in the disordered phase to a discrete set of symmetries in the ordered phase.

Fig. 1.2 shows a system which demonstrates rotational symmetry breaking. An example would be a magnetic material where the arrows indicate the local magnetic moment of the material. Again, since the direction of the arrows is random in the disordered phase, when the system is rotated there is no distinction between the original and rotated states i.e., the directions will still be random. In the ordered phase, however, any rotation in the plane other than a full 360° rotation will change the common direction of the arrows. A rotation around

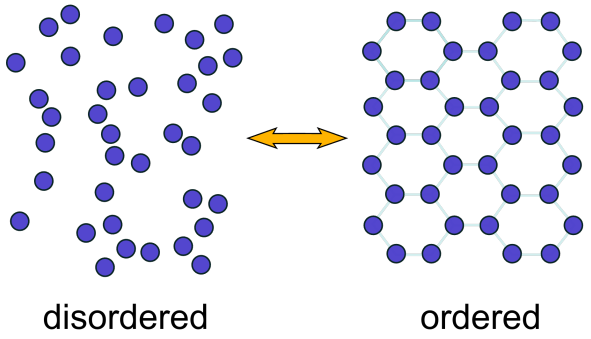

Figure 1.1: Two phases distinguished by translational symmetry breaking. In the disordered state, the statistical ensemble describing the state has continuous translational symmetry because the particles are randomly distributed. In the ordered phase this is no longer the case, as the crystal structure requires the particles to be translated into specific positions in order for such a translation to be a symmetry.

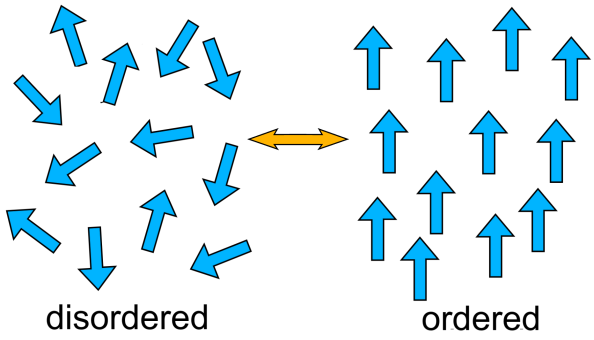

Figure 1.2: Two phases distinguished by rotational symmetry breaking. Arrow positions are ignored for this example. In the disordered state, the statistical ensemble describing the state has rotation symmetry in all three dimensions because the arrow directions are randomly distributed. In the ordered phase this is no longer the case, as the arrows have a common direction.

an axis parallel to the common direction will remain a symmetry. In this case this would be a rotation around the vertical axis. Therefore, the symmetry of the system has been reduced from a full set of rotations in the disordered phase to the smaller set of rotations around the vertical axis in the ordered phase.

In this paradigm, we can introduce the idea of a *local order parameter*, a quantity which is locally defined but constant across the system and whose value determines the phase. For the system in Fig. 1.2, one can take the average of all arrows in a small region. In the disordered phase, the ensemble average of this quantity is zero since the directions of the arrows are

random. In the ordered phase, it is nonzero and points along the common direction of all arrows. Thus, this order parameter distinguishes the phases. Note that although the order parameter is local, only including arrows near a specific point, its value is identical at all points in space.

1.1.2 Topological Invariants

As powerful as the symmetry breaking paradigm is, it cannot describe phases which are not distinguished by a local order parameter. Such an example is found in quantum systems, where certain quantum phases are distinguished by a topological order parameter. Topology is a field of mathematics that deals with the connectedness and large-scale properties of objects. The standard example is to consider the difference between a sphere and a torus. There is a clear invariant that separates them: the torus has one hole, while the sphere has none. In technical terms, the sphere is a genus 0 surface while the torus is a genus 1 surface. Any small region of a surface, though, does not have enough information to determine the genus; one must examine the entire object. In other words, no local quantity can distinguish the two, and one must consider the entire surface to make the distinction. Furthermore, the genus must be an integer, which has the consequence that a sphere cannot smoothly deform into a torus. If a sphere were to be deformed into a torus, then there must be at least one specific point in the deformation where the genus changes from 0 to 1[1]. These *topological invariants*, such as the genus of a surface, can be used to differentiate certain quantum phases of matter. The point where such an invariant changes from one value to another will indicate a phase transition between them. Thus, these phases are described by *nonlocal*, topological order parameters.

However, unlike our sphere and torus analogy, the topological nature of these systems is generally something more abstract. Let us discuss one of the earliest examples, the Thouless-Kohmoto-Nightingale-den Nijs (TKNN) invariant [17]. This was originally applied to the

[1]More precisely, there must be a point where the genus is degenerate - the number of holes cannot be defined. This is the point where the genus can change from 0 to 1.

Integer Quantum Hall Effect (IQHE) [18], but more generally explains topological phenomena in a class of materials called Chern insulators [19].

A description of the IQHE follows. When a magnetic field is applied in a perpendicular direction to a current, there is a voltage in the direction perpendicular to both the current and the magnetic field. This is the classical Hall effect which can be explained by the magnetic Lorentz force acting on the charge carriers in the conductor. This voltage can drive a current and has an associated conductance, σ_{xy}. In 1980, it was discovered that the Hall conductance is quantized in exact multiples of e^2/h in a two-dimensional conductor with a magnetic field applied perpendicular to the plane of the conductor [18].

This quantization can be explained in terms of a topological order parameter. The Brillouin zone[2] of the conductor is a two-dimensional electron state space, where each electron quantum state is identified with a two-dimensional crystal momentum, $\vec{k}$. The Brillouin zone is finite, with periodic boundaries. It has a size that is determined by the atomic spacing in the material containing the electrons. In the limit of infinite conductor size, the Brillouin zone is a continuous space, and one can study the behavior of electronic wavefunctions which are localized around some crystal momentum $\vec{k}$.

Because each point of the Brillouin zone represents a quantum state, there is a subtlety in these localized wavefunctions. As the electron state moves along a path Γ within the Brillouin zone, it will pick up an overall complex phase

$$e^{-i\theta} = e^{-\int_\Gamma \langle k|\vec{\nabla}_k|k\rangle \cdot d\vec{l}}. \tag{1.1}$$

This complex phase $e^{-i\theta}$ is called the *geometric phase* or *Berry phase*. This phase reflects the properties of the system that give rise to a nontrivial connection between nearby points of the Brillouin zone. This is mathematically very similar to the Aharonov-Bohm phase, which affects electron wavefunctions in real space within the vicinity of a magnetic field.

The topology is manifested when we consider the phase accrued by an electron wavefunc-

[2]When a magnetic field is present as in the case of the IQHE, one technically uses a slight modification called the magnetic Brillouin zone. This will not affect the discussion.

tion as it traverses a closed path Γ. In such a case, the line integral can be turned into a surface integral by Stokes's theorem[3]. Because the Brillouin zone is closed and has periodic boundary conditions, there are two choices for this surface integral. Both integrals must give the same complex phase $e^{-i\theta}$ since they represent the same physical quantity. However, because the integral occurs in the exponent, the surface integrals can differ by an integer multiple of 2π and the complex phases will agree. This is where the topological nature of the TKNN invariant first manifests. The fact that the Brillouin zone is closed is a global property that allows for the existence of two surface integrals, and the nature of complex phases allows the two integrals to disagree by $2\pi n$ for $n \in \mathbb{Z}$.

Now consider the limit as the path Γ expands to become the perimeter of the Brillouin zone. This path encircles the full area of the Brillouin zone. It is still considered to divide the Brillouin zone into two surfaces, but one of those surfaces has zero area. The surface integral corresponding to this is trivially zero, implying that the complex phase is equal to 1. Thus, $e^{-i\theta} = 1$ and we are left with the result

$$\theta = -i \oint_{\Gamma} \langle k|\vec{\nabla}_k|k\rangle \cdot d\vec{l} = 2\pi n \tag{1.2}$$

for $n \in \mathbb{Z}$. This value n in this context is known as the TKNN invariant. Through a linear response equation known as the Kubo formula, this value n is shown to be directly related to the Hall conductivity in the IQHE. In particular, the Hall conductivity σ_{xy} is given by

$$\sigma_{xy} = \frac{e^2 n}{h}. \tag{1.3}$$

The unique aspect of this analysis is that the quantization of n into integer values relies crucially on the topology of the Brillouin zone. Looking at the behavior of an electron wavefunction in a small region of the Brillouin zone will not contain the necessary information to calculate this quantity. This makes it fundamentally different from the symmetry breaking phases, which have local order parameters. In addition, the nonlocal nature of this quantity

[3]Assuming that the path has trivial homology i.e., it does not wrap around the Brillouin zone's periodic boundaries.

makes it robust to disorder and perturbation. A small perturbation cannot change n by a small amount, as n must be an integer. This is what allows us to call it an invariant.

In the years following the discovery and explanation of the Integer Quantum Hall Effect, many other quantum phases were discovered that relied on the topology of quantum states; the Quantum Anomalous Hall Effect, topological insulators, Weyl semimetals, and symmetry-protected topological phases are all prominent examples. In more general cases such as these, it can be convenient to define topological order through quantum entanglement.

There is an understanding that topological order is contained in the long-range entanglement properties of a system. Topological properties are not changed by any local action, and thus one would expect that applying a finite number[4] of local quantum unitary operations to a state will preserve its topological order [20]. This can be used as a definition of a topological phase. The trivial product state is clearly topologically trivial, and thus every state that can be mapped to the trivial product state by a finite number of unitary operations is a topologically trivial quantum state (by definition). Such local unitary actions can only entangle locally, and thus a topologically trivial state can only have local, or "short-range" entanglement. This leaves topological states to have a long-range entanglement which the local actions cannot remove nor create. In this sense, the topological properties of a system depend on the nature of its quantum entanglement. The idea that entanglement can distinguish phases will continue to appear in the examples that follow.

1.2 Nonequilibrium Phases

Though the examples of the previous section had a variety of differences, they had the common property of being considered equilibrium phases. That is, the defining properties of these systems are manifested while the systems are in thermodynamic equilibrium. By removing

[4]Here, we group unitary operations that do not overlap into one operation called a layer. The precise statement here is that in the limit of infinite system size, the number of layers necessary for this procedure remains constant and is thus independent of system size.

this requirement, one can probe *nonequilibrium phases*, also called *dynamical phases*. In these, the system does not reach thermodynamic equilibrium; and even if the system reaches a steady state, there is often some nonzero flux of energy through the system.

One example of a nonequilibrium phase is the quantum *many body localized* (MBL) phase. The MBL phase is an interacting phase of matter where an initially nonequilibrium state will not relax to equilibrium as otherwise expected[5]. Quantum systems which do relax to thermal equilibrium, called *ergodic* states, exhibit the behavior expected from the eigenstate thermalization hypothesis (ETH). This hypothesis states that if such an ergodic system is initially in a physical[6] nonequilibrium state then that state will, after a long enough time, evolve into a state in which observables appear thermal and information about the initial state is lost [21]. One expects that at late times, quantum correlations present in the initial state are spread across the system in an inaccessible way. Thus, time averaged expectation values of local observables can be described as they are in statistical mechanics, in terms of microstates and macroscopic conserved quantities such as particle number and total energy.

The MBL phase describes a type of quantum system which does not conform to the eigenstate thermalization hypothesis. Specifically, it is a perfect interacting insulator at a nonzero temperature [22]. This can be explained in terms of competition between two opposing behaviors. There exist localization phenomena that tend to constrain degrees of freedom while thermalization tends to spread and dilute information across the system. A many body localized system exhibits strong localizing behaviors that are supported by many body dynamics. From this it follows that energy cannot spread easily across the system, and this is characteristic of an insulator. An ideal MBL state is a perfect insulator and the system cannot exchange particles and energy between regions, which prevents the system from reaching thermal equilibrium. As a result, a nonequilibrium state which is in the MBL phase will never reach thermodynamic equilibrium, even after an infinite amount of time.

---

[5]Specifically, the state does not thermalize for a very long time, parametrically long in system size.

[6]i.e., a state that can be reasonably prepared in an experiment. Specifically, we are excluding any individual many-body excited eigenstates, which are themselves stationary states.

In fact, such systems resist thermalization even when driven by an external driving force, which is normally expected to heat the system.

The conflict between the two opposing behaviors can also be seen in how MBL phases have distinct entanglement properties. This is quantified in "volume-law" and "area-law" behaviors, which will be fully introduced in Sec. 1.3.1. For an ergodic system, thermalization and information spreading suggest that eigenstates with a finite nonzero energy density will have entanglement scaling that follows a volume-law. MBL systems in contrast tend to have strong localizing behaviors and demonstrate entanglement scaling that follows an area-law. This key observation, that localization can change the entanglement characteristics of a system, will be an important concept moving forward.

Another example of a nonequilibrium phase is that of a Floquet topological phase. A Floquet system is one which is driven by some periodic external force; as such, there is a nonzero flux of energy at all times. Floquet systems are able to support topological phases that are impossible in an equilibrium setting [23]. This is possible in large part due to the fact that Floquet systems can conserve *quasienergy*. In the same way that spatial periodicity leads to a conserved periodic crystal momentum, temporal periodicity leads to a conserved periodic quasienergy, and this allows for the formation of novel band structures. The difficulty of experimentally probing Floquet states of matter lies in the fact that a driving force tends to add energy to the system. At long times, this thermalizes the system, increasing local entropy density, and leading to a featureless state which prevents observation of relevant quantum effects [23]. Experiments can combat the problem of thermalization by focusing on short time scales, and using driving frequencies that are much larger than the relevant energies of the system so as to prevent transitions between states. From a theoretical perspective, one way to combat this is to focus on free (i.e., non-interacting) fermionic systems. In the limit of weak interactions, fermionic systems have an extrinsic number of conserved quantities, namely the fermion occupation numbers. Even in interacting fermion systems, one can expect to find systems where there are a large number of conserved quantities, and this prevents thermalization. In addition, one can look for nonthermalizing regimes such as the

proposed Floquet MBL phases.

1.3 Measurement-Induced Quantum Phases

The previous examples of nonequilibrium phases have demonstrated the following important aspect of such phases: driven or interacting systems tend to quickly thermalize, and interesting nonequilibrium phases need a mechanism that prevents this, such as localization. It was recently realized that projective measurements can serve as a novel source of localization [24, 1]. For example, the measurement of a particle occupation number collapses the wavefunction and may localize the particle to a single site, depending on the measurement outcome. It has now been shown that this source of localization is sufficient to prevent thermalization and stabilize a nonequilibrium phase. This novel nonequilibrium phase is known as a *measurement-induced quantum phase*.

The simplest examples of systems which exhibit a measurement-induced quantum phase involve systems subjected to unitary evolution along with regular projective measurements. A hallmark of such a phase is the nature of the system entanglement. Unitary evolution tends to entangle degrees of freedom across the system, while projective measurements tend to disentangle degrees of freedom. The system can then exhibit an "area-law" or "volume-law" entanglement depending on which factor is stronger, and this indicates different phases of the system. A definition of area-law and volume-law behaviors will be given in Sec. 1.3.1.

Phases of this type will be the focus of the remainder of this introduction. The primary concepts will be introduced by first looking at a concrete example. The following is a description of one of the earliest examples of a measurement-induced quantum phase, as described by Li, Chen, and Fisher in Ref. [1]. A diagram of the setup is given in Fig. 1.3. There is a one-dimensional chain of N qubits i.e., bosons with a two-dimensional local Hilbert space. The dynamics of the system are split into time steps, which are applied sequentially to our system. At odd time steps, a random two-qubit unitary gate is applied to pairs of qubits, as shown in the diagram. There is choice in the random probability distribution. The Haar random distribution over all possible two-site unitary gates is the most general

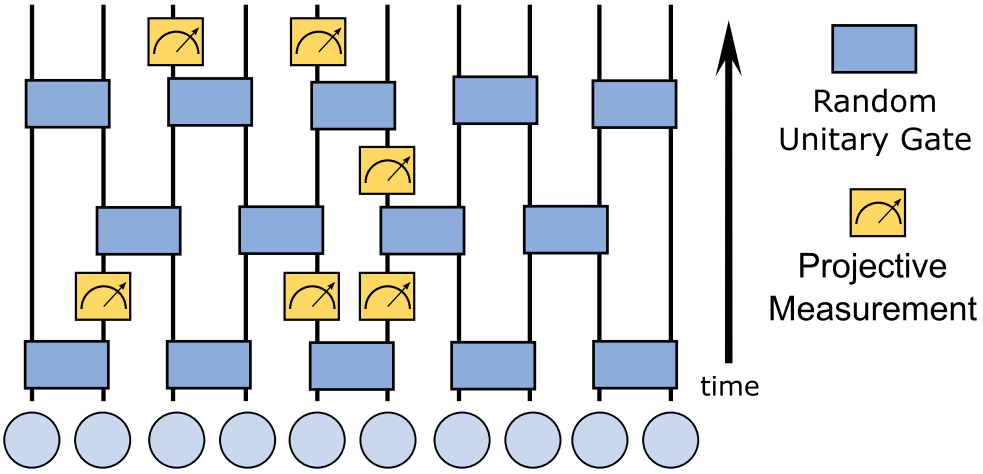

Figure 1.3: A diagram of the dynamical procedure in Ref. [1]. The vertical lines represent the worldlines of qubits (represented by circles at the bottom of the diagram), and the boxes depict operations being applied to the qubits over time. The blue boxes are two-qubit unitary transformations, and the yellow boxes are single-qubit projective measurements. Notice that the pairing of the qubits for the unitary gates alternates at each time step, leading to a "bricklayer" pattern of blue boxes.

choice, and a uniform distribution over all two-site Clifford unitary gates is also common. The Clifford unitaries are often chosen to improve computational efficiency, as described in Ch. 2 of this thesis.

After applying the unitary gates, the system is subjected to projective measurements. Each qubit is measured with a probability p. This measurement will project the qubit into an independent state determined by the Born probability of the measurement and it will no longer be entangled with the rest of the system. At even time steps, random two-qubit unitary gates are again applied to the alternate pairing of qubits. Afterwards, each qubit is again measured with probability p.

There are two independent sources of randomness in this procedure. The first source

comes from the application of the operations, as there is randomness in what is applied and where it is applied. The second source comes from the inherent randomness of quantum measurement contained in the Born probability. Because of this randomness, one works with an ensemble of states. Starting with an identical initial state, many realizations are made using the procedure and each system will evolve into a different final state. Quantities such as entanglement are averaged over this ensemble. Note that the states are exactly known at all times. Therefore, this is an ensemble of quantum trajectories, and not a statistical ensemble.

The two operations, unitary evolution and projective measurement, create a form of frustration in the system. The unitary gates tend to entangle qubits with each other, and as more are applied, the system entanglement increases. The measurements tend to remove entanglement from the system, since the measured particles can no longer be entangled with the rest of the system. There is competition between these two elements, and a higher probability of measurement p will lead to less entangled systems. More specifically, the expectation is that after a long enough time the system will reach a steady state (though not necessarily a thermal state) where these two forces balance each other. Then the entanglement will not significantly change over time and only undergo small fluctuations. In this steady state, dynamics with a larger value of p will result in less entangled systems.

This can be most easily seen in the extreme cases of $p = 0, 1$. For $p = 0$, no measurements are applied, and the unitary gates should result in a system that is maximally entangled. For $p = 1$, every site is measured at every time step and this removes all entanglement. Therefore it is expected that the entanglement will decrease as p increases. What is less obvious, however, is that the *nature* of this entanglement, as defined in the next section, should change dramatically at a specific value of p.

1.3.1 Subsystem Entanglement

To identify a change in the nature of entanglement, one must first specify a measure of entanglement for the system. Given some region A of the system and its complement $\bar{A}$,

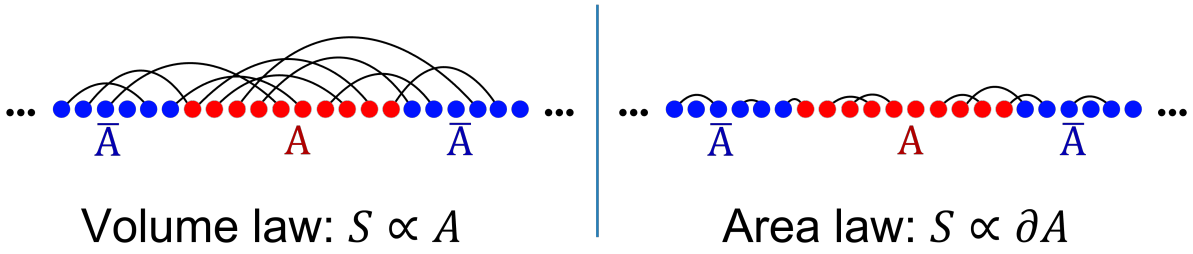

Figure 1.4: Caricature of an entangled quantum system, illustrating the difference between volume-law and area-law entanglement scaling. The circles are qubits, and the lines represent entanglement between qubits. The volume-law system has qubits entangled at all distances, so the total entanglement between a region A and the rest of the system will be proportional to the total number of qubits in A. The area-law system has qubits entangled over short distances, so the entanglement between A and $\bar{A}$ will only depend on qubits near the interface between the two regions.

the *subsystem entanglement entropy* $S(A)$ gives a measure of the entanglement between A and $\bar{A}$. Mathematically, this is a function of the reduced density matrix of A, as described in Sec. 2.6.1. One way this can be used to probe the character of the entanglement in a system is to see how $S(A)$ varies with the size of A. If $S(A)$ is proportional to the volume of the region A, we say that the entanglement entropy has a volume-law behavior. However, if $S(A)$ is proportional to the area of the boundary between A and $\bar{A}$, we say that the system has an area-law behavior. In general, we can think of volume-law systems as having greater entanglement, and more long-range entanglement, than area-law systems.

The motivation for this is shown in Fig. 1.4. In this caricature of a one-dimensional entangled quantum system, only two particles are entangled at any given time, and the entanglement between each entangled pair is identical to every other pair. Colored circles represent the qubits of the system, and black lines connect entangled qubits. The subsystem entanglement entropy $S(A)$ is given by the number of lines connecting the region A with

the rest of the system $\bar{A}$. The right side of Fig. 1.4 shows a system that has an area-law behavior of entanglement scaling. The qubits are generally entangled with nearby qubits. As the region A grows in size, the subsystem entanglement entropy will only depend on the entanglement of particles that are near the border between A and $\bar{A}$. Since the entanglement entropy is proportional to the size of the boundary, we call this an area-law behavior. In the case of one dimension, this means that $S(A)$ will approach a constant value as the size of A increases because the "area" of a one-dimensional region A consists only of its two endpoints.

The system on the left side in Fig. 1.4 shows a system that has a volume-law behavior of entanglement scaling. We see that in this system, entangled pairs of particles can be separated by any distance. Therefore, as we increase the size of A, the subsystem entanglement entropy is expected to have some contribution from many particles inside of the region, and not only those near the boundary. Therefore, $S(A)$ is proportional to the "volume" of the region A, which is the length of the one-dimensional subsystem.

Turning back to the system of unitary gates and projective measurements, both volume-law and area-law behaviors are expected. For $p = 0$, the unitary gates will lead the system to a maximally entangled volume-law state. For $p = 1$, the entanglement is removed at the end of each time step; therefore the subsystem entanglement entropy is a constant, namely zero. Thus, it is considered an area-law state. The volume-law and area-law behaviors are drastically different, and it would be reasonable to believe that the system cannot smoothly transition from one behavior to the other as p is varied. Rather, there might be a special point, a critical value of p, that separates the volume-law dynamics from the area-law dynamics.

This is what is found when the system is simulated. There is a critical point, at approximately $p_c \approx 0.16$, where for values $p < p_c$, the system shows volume-law entanglement scaling, and for values $p > p_c$, there is area-law entanglement scaling. At the critical point p_c, the system is neither volume-law nor area-law entangled, but is rather in a critical phase that has *logarithmic-law* entanglement scaling. That is to say that the entanglement entropy $S(A)$ is proportional to the logarithm of the subsystem size.

1.3.2 Purification Transitions

The behaviors of these measurement-induced phases are relevant to quantum computation efforts. If the system is meant to model quantum memory, then the measurements can be interpreted as disturbances from the outside. While it is always a goal to reduce such noise, these results imply that there may be a critical rate of noise where the effects on the quantum memory change drastically. To study this, however, it is more appropriate to focus on the *purity* of the system instead of the subsystem entanglement entropy.

In quantum mechanics, uncertainty can be broadly separated into two categories. The first comes from inherent quantum uncertainties arising from quantum superpositions. The second is the more familiar uncertainty arising from a lack of knowledge about a system. It is important to understand this distinction. If we know the exact quantum state of a particle, then it may still be impossible to know beforehand the outcome of a measurement. This is due, however, to quantum effects and not a lack of knowledge, because we knew exactly the quantum state of the particle before it was measured. Furthermore, superpositions can hold quantum information e.g., through quantum correlations between particles, while clearly no information is held in one's lack of knowledge about a quantum system. A quantum system whose state is exactly known is said to be in a *pure* state while a *mixed* state describes a system where full information is not available.

While investigating measurement-induced phase transitions, it was discovered that there can also exist phase transitions in the purity of a system [4]. The setup for such a system is similar to what was discussed above. An ensemble of identical systems is prepared and subjected to hybrid dynamics of unitary operations and projective measurements. The initial systems, however, are each a mixed state that has an incomplete description. There is competition between the two elements of the dynamics: when measurements are taken and their results recorded they tend to reveal information about the state and increase the purity, while the unitary operations spread the information across the state and make it more difficult to extract via local measurements. In addition, much like the entanglement transitions, it

has been observed that there are certain systems in which the behavior of the system purity will undergo a phase transition as the rate of measurements is increased past a critical value. For a small rate of measurement p, a large number of measurements are required to extract all quantum information from the system. In this case, the number of measurements is exponential in system size. For a large rate of measurement, the system purifies completely after a number of measurements comparable to system size.

This has immediate consequences for quantum computing. In such a model, the system can be seen as a quantum memory, and the measurements act as external noise. In the theoretical models, the observer takes the role of an outside interfering force. Therefore, in the "mixed" phase at low measurement rates, the quantum information is preserved since the external observer cannot extract the system's information until after an exponential amount of time. Therefore, these results imply that there is a critical rate of noise, after which the noise becomes far more destructive to the state, and the system will no longer be able to effectively protect its quantum information from the external actions [4, 8].

1.3.3 Outline

The work in this thesis involves simulating quantum systems which exhibit these measurement-induced phases. In general, quantum systems are difficult to simulate on classical computers, especially systems with a large amount of entanglement. This is due in large part to the exponential nature of the state space of a quantum system. For N particles which each have d internal degrees of freedom, the Hilbert space is a d^N-dimensional complex vector space. We would generally need on the order of $2d^N$ real numbers to define our state, and this number is prohibitively large for classical computers. Thus, various methods have been invented that allow efficient simulations of certain classes of quantum systems. We focus on two of these methods.

The first method is called the *stabilizer formalism*. In this method, a quantum state is defined implicitly by a set of Hilbert space operators called Pauli strings. These Pauli strings can be specified with a relatively small amount of information, and so allow us to efficiently

simulate systems where the quantum state can always be described by these Pauli strings.

The second method is called the *Gaussian state formalism*. A Gaussian state of a system of fermions can be completely described by the two-point correlation function of the state. The Gaussian formalism takes advantage of this to efficiently represent Gaussian states for computation. Free fermion operations and certain measurements will preserve the Gaussian property of a state, and this can be used to simulate a free fermion evolution and measurement with a numerically tractable computation.

The following is an outline of each of the thesis's chapters. In Ch. 2, we look at bosonic systems using the stabilizer formalism. We review the formalism, and use it to implement a generalization, such that the on-site Hilbert space dimension can be increased from $d = 2$ to any prime number d. We then give the results of simulations involving prime d and show that the phase transitions persist, while also extracting exponents which characterize the transitions. In Ch. 3, we work with fermionic systems through the framework of Gaussian states. We review the Gaussian state formalism and define a system with an exact mapping to a classical statistical mechanics model with a known phase transition. We then generalize this system and find that the phase transition persists. The transition is between phases which are qualitatively similar to the statistical mechanics model, however certain symmetries become lifted and enable phase transitions where there previously were none.

Chapter 2

BOSON STABILIZER ENTANGLEMENT TRANSITIONS

In this chapter, we discuss the simulation of measurement-induced phase transitions using the stabilizer formalism. In particular, while the transition has been seen many times for qubits (i.e., systems composed of many two-level systems), we will characterize the phase transition for qudits (i.e., systems composed of many d-level systems), when the on-site Hilbert space dimension is a prime number. We introduce a generalization [14, 15] which allows us to take the Pauli stabilizer formalism most often introduced for qubit systems and apply it to a qudit system. With this formalism, we can apply a circuit of Clifford unitary gates and projective measurements to a system of qudits, and study both the entanglement properties and purity properties as a function of time.

For $d = 2$, it has been shown that there is both a measurement-induced entanglement transition [1] and a measurement-induced purification transition [4] at the same critical rate of measurement. It has been shown analytically that for circuit with completely random (i.e., Haar random) unitary gates, the transition persists and the critical rate of measurement p_c should increase with d. The primary analytical result from these previous studies is that in the limit $d \to \infty$, the phase transition occurs at $p_c = 0.5$ and is described by the 2D percolation transition [25, 26]. Apart from this limit, little progress has been made in analytically understanding the entropy of these systems [27]. It is known that the percolation universality class does not describe the transition at finite d. In addition, these results do not necessarily extend to Clifford circuits, and the behavior of these circuits at finite d has not been studied in depth.

We show that for certain prime d, these phase transitions persist. For all d we study, we find that entanglement transitions can be characterized by the correlation length critical

exponent $\nu \approx 1.3$, which is close to the value of the percolation critical exponent $\nu = 4/3$. This is interesting as the universality class of Clifford circuits is not expected to be the same as that of Haar random circuits [25]. Furthermore, although the true Clifford universality class has not been identified, our results support the idea that Clifford transitions share the same critical exponent ν for various values of d. We find that the critical value p_c increases with d, which agrees with the analytic result, and we can study how the value approaches the $d = \infty$ limit. In addition, we find that for every value of d we studied, a purification transition exists and occurs at the same critical value as the entanglement transition.

2.0.1 Description of Model

The dynamical setup we consider is shown in Fig. 2.1. We study a one-dimensional chain of N qudits of prime order d with periodic boundary conditions. At each time step, we apply random Clifford unitary gates to pairs of neighboring sites and perform projective measurements with probability p at each site.

To study the entanglement transition, we start with a trivial product state and apply the above dynamics for enough time steps that the system reaches a steady state. This steady state is the point at which the quantities described below are relatively constant, and do not evolve in time with the exception of small fluctuations. We then calculate the following two quantities: the bipartite subsystem entanglement entropy $S(L)$ averaged over all subsystems of length $L \leq N$, and the *normalized stabilizer length distribution* $D_{\mathcal{G}}(L)$ as defined in Sec. 2.6.3 below. This is repeated for various values of measurement probability p, and the values of these two quantities reveal the existence of two quantitatively distinct phases at different values of p: a volume-law phase and an area-law phase.

To study the purification transition, we start with a completely mixed state and apply the above dynamics for N time steps, where N is the size of the system. This models a system in which the measurement results are recorded, and thus the statistical uncertainty of the system decreases with time. We then measure the entropy of the mixed state, which is inversely related to the statistical certainty of the state, also known as the purity. This is

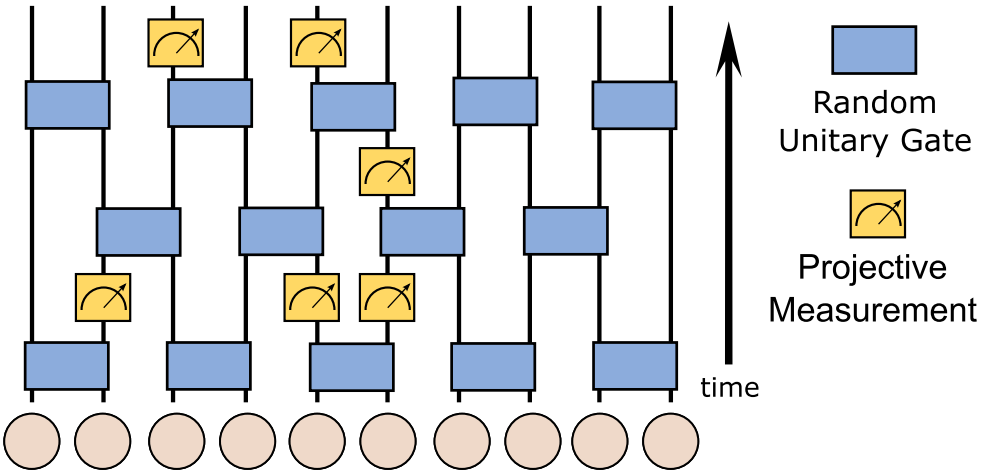

Figure 2.1: A diagram of the dynamics that are studied throughout this chapter. The system is a one-dimensional chain of qudits. This circuit diagram represents the history of the quantum state, with time increasing in the vertical direction and vertical lines representing individual qudits. The blue boxes are two-site Clifford unitary gates which are chosen randomly using a uniform distribution over all possible Clifford gates. The yellow boxes are single-qudit projective measurements onto the generalized Pauli Z eigenbasis as described in the text, and are applied with probability p to every qudit between applications of Clifford gates. The pairing of sites for the two-site unitary gates alternate, and one time step is defined to include two layers of unitary gates so as to include both possible pairings.

repeated for various values of p. This shows the existence of two phases: a purifying phase where the system becomes a pure state within a time scale of order N, and a mixed phase where the system purifies on time scales much longer than N.

The structure of this chapter is as follows. First, in Sec. 2.1 we introduce the stabilizer formalism as applied to qubits. This demonstrates how states can be efficiently represented using this formalism, and introduces a class of unitary transformations called Clifford operations. In Sec. 2.2 we introduce the extension to qudits, which have a d-dimensional on-site Hilbert space. We explain the differences between this extension and the previous $d = 2$ case. This shows that states can be efficiently represented in much the same way for any value of d. In Sec. 2.3 we outline some of the algebraic properties of the stabilizer representation. In particular, commutation requirements of stabilizer operators can be encoded into a symplectic vector space, and Clifford operations performed on the state are represented by symplectic matrices. In Sec. 2.4 we demonstrate a method for finding a random symplectic matrix, which itself is the representation of a random Clifford unitary acting on our system. In Sec. 2.5 we introduce a tool for extracting data from our state, called the "clipped gauge." In Sec. 2.6 we explain how to use the clipped gauge to calculate the key quantities used to describe the system, namely the subsystem entropy, purity, and the normalized stabilizer length distribution. Finally, we produce our results in Sec. 2.7, in which we characterize the phase transitions for systems of qudits with $d = 3$, 5, and 97.

2.1 Quantum Bits

The first section of the chapter is dedicated to reviewing the stabilizer formalism as applied to qubits. For more information, see Ref. [28]. The significance of the stabilizer formalism is that a certain class of quantum states called *stabilizer states* on N qubits can be described by an $N \times 2N$ matrix of integers modulo 2. This is drastically better than the direct description of the state wavefunction, which would require 2^N complex numbers.

We will consider a one-dimensional system of N qubits. This system will have a Hilbert space of dimension 2^N, being the tensor product of the local two-dimensional qubit Hilbert

spaces.

On a single qubit space, there are three important operators called the *Pauli matrices*:

$$X = \begin{pmatrix} 0 & 1 \\ 1 & 0 \end{pmatrix} \qquad Y = \begin{pmatrix} 0 & -i \\ i & 0 \end{pmatrix} \qquad Z = \begin{pmatrix} 1 & 0 \\ 0 & -1 \end{pmatrix} \tag{2.1}$$

All three are unitary and hermitian matrices which square to the identity matrix. All three mutually anticommute, and the product of any two will be another Pauli matrix (or the identity I), up to a factor of $\pm i$.

2.1.1 Stabilizers

A *Pauli string* is an operator of the 2^N-dimensional Hilbert space which is a tensor product of one Pauli matrix (or I) for each site in our system, with an additional overall factor of ± 1 or $\pm i$. Since the product of Pauli matrices is another Pauli matrix or the identity, the set of all Pauli strings is closed under multiplication, and thus this set is a group. The *Pauli group* on N qubits, $\mathcal{P}_N^2$, is the set of all Pauli strings. Since $Y = iXZ$, we can use the Pauli matrices X and Z as a basis to write any Pauli string in the form $g = (i)^{b_1}(-1)^{b_2} X_1^{a_1} Z_1^{a_2} X_2^{a_3} Z_2^{a_4} ...$, with $b_j, a_j \in \{0, 1\}$. Here, $X_j = I \otimes ... \otimes X \otimes ... \otimes I$ is the Pauli X operator acting on site j and acting as the identity at all other sites. Note that since Pauli matrices at the same site anticommute, Pauli strings will either anticommute or commute depending on the number of sites that share anticommuting Pauli operators.

A subgroup $\mathcal{S}$ of $\mathcal{P}_N^2$ is a *stabilizer group* if there is some subspace $V_\mathcal{S}$ of our Hilbert space such that for every element $g \in \mathcal{S}$ and for all vectors $|\psi\rangle \in V_\mathcal{S}$, we have $g|\psi\rangle = +|\psi\rangle$. Since Pauli strings either commute or anticommute, we see that the elements of $\mathcal{S}$ must all mutually commute, since they share a +1 eigenvector. If this were not true for two elements g and h, it would lead to the contradiction $|\psi\rangle = gh|\psi\rangle = -hg|\psi\rangle = -|\psi\rangle$. In addition, $-I$ cannot be an element of the stabilizer group, since it only has -1 as an eigenvalue. These two conditions are both necessary and sufficient for a subgroup $\mathcal{S} \subset \mathcal{P}_N^2$ to be a stabilizer group.

In practice, the stabilizer group is almost always described by a generating set, $\mathcal{G}$. A generating set is a subset of $\mathcal{S}$ such that every element in $\mathcal{S}$ can be written as a product of elements in $\mathcal{G}$. These elements are called generators, and are said to generate the set $\mathcal{S}$. We will usually focus on minimal generating sets, which have the smallest number of generators possible while still generating $\mathcal{S}$. These have generators which are independent, in that no generator in $\mathcal{G}$ can be written as a product of other generators in $\mathcal{G}$, otherwise it would be a redundant generator. This has the immediate consequence that each stabilizer in $\mathcal{S}$ is a *unique* product of elements in $\mathcal{G}$. If this were not true, and there were to exist some element g for which $g = g_1 g_2 ... g_M = g'_1 g'_2 ... g'_N$ for some generators g_i and g'_j, then we would have $g_1 = g'_1 g'_2 ... g'_N g_M^{-1} ... g_2^{-1}$, contradicting the independence of the generators. Note however that the smallest generating set is not unique. There will be many subsets of $\mathcal{S}$, whose elements are independent of other elements in that subset, that have the same number of generators.

All Pauli strings square to the identity matrix, up to a factor of ± 1. Since all stabilizers have a $+1$ eigenstate, $g^2 = +I$ for stabilizers. This means that we can write any element $g \in \mathcal{S}$ as $g = (g_1)^{a_1}(g_2)^{a_2}(g_3)^{a_3}...$, where $g_i \in \mathcal{G}$ and $a_i \in \{0, 1\}$. The order of the terms does not matter, since all of the stabilizers mutually commute. All stabilizers can be written as such a product, and all such products are valid stabilizers. Since we have already shown that each such combination must also be unique, we see that for such a minimal generating set, $|\mathcal{S}| = 2^{|\mathcal{G}|}$. Furthermore, all stabilizer groups must contain 2^k elements for some integer k.

The size of $\mathcal{G}$ is directly related to the size of our stabilized subspace $V_{\mathcal{S}}$. We show this by first introducing the projector $P_{\mathcal{S}}$ onto $V_{\mathcal{S}}$ and then using the fact that $\dim(V_{\mathcal{S}}) = \mathrm{Tr}(P_{\mathcal{S}})$ for projectors. The projector is given by

$$P_{\mathcal{S}} = |\mathcal{S}|^{-1} \sum_{g \in \mathcal{S}} g. \tag{2.2}$$

First, we prove that this is a projector by showing $(P_{\mathcal{S}})^2 = P_{\mathcal{S}}$:

$$\begin{aligned} P_{\mathcal{S}} P_{\mathcal{S}} &= |\mathcal{S}|^{-2} \left(\sum_{g \in \mathcal{S}} g \right) \left(\sum_{g' \in \mathcal{S}} g' \right) = |\mathcal{S}|^{-2} \sum_{g \in \mathcal{S}} \left(\sum_{g' \in \mathcal{S}} g \cdot g' \right) \\ &= |\mathcal{S}|^{-2} \sum_{g \in \mathcal{S}} \left(\sum_{g'' \in \mathcal{S}} g'' \right) = |\mathcal{S}|^{-2} |\mathcal{S}| \left(\sum_{g'' \in \mathcal{S}} g'' \right) = P_{\mathcal{S}}, \end{aligned} \tag{2.3}$$

where the second line follows from the group theory result that $\phi_g(h) = g \cdot h$ is an isomorphism of $\mathcal{S}$.

This projector has the required property that all vectors in the projected subspace (i.e., vectors $|\psi\rangle$ such that $P_{\mathcal{S}}|\psi\rangle = |\psi\rangle$) are +1 eigenstates of elements in the stabilizer group:

$$g|\psi\rangle = gP_{\mathcal{S}}|\psi\rangle = g\left(|\mathcal{S}|^{-1}\sum_{g'\epsilon\mathcal{S}} g'|\psi\rangle\right) = |\mathcal{S}|^{-1}\sum_{g'\epsilon\mathcal{S}} g\cdot g'|\psi\rangle = |\mathcal{S}|^{-1}\sum_{g''\epsilon\mathcal{S}} g''|\psi\rangle = P_{\mathcal{S}}|\psi\rangle = +|\psi\rangle$$

Finally, we can calculate the dimension of $V_{\mathcal{S}}$ by taking the trace:

$$\mathrm{Tr}(P_{\mathcal{S}}) = \mathrm{Tr}\left(|\mathcal{S}|^{-1}\sum_{g\epsilon\mathcal{S}} g\right) = |\mathcal{S}|^{-1}\sum_{g\epsilon\mathcal{S}}\mathrm{Tr}(g) = |\mathcal{S}|^{-1}2^N = 2^{N-|\mathcal{G}|}$$

This follows from the fact that for a tensor product, $\mathrm{Tr}(A\otimes B) = \mathrm{Tr}(A)\mathrm{Tr}(B)$. All of the Pauli matrices are traceless, and so the only term to contribute to the sum is $\mathrm{Tr}(I) = 2^N$. Therefore, a stabilizer group of size $|\mathcal{S}| = 2^{|\mathcal{G}|}$ will stabilize a subspace of dimension $2^{N-|\mathcal{G}|}$.

It is also convenient to point out that the projector $P_{\mathcal{S}}$ can be written entirely in terms of a generating set $\mathcal{G}$. This is a consequence of the fact that every stabilizer can be written in the form $g = (g_1)^{a_1}(g_2)^{a_2}(g_3)^{a_3}... = \prod_{g_i\epsilon\mathcal{G}}(g_i)^{a_i}$ for some exponents a_i:

$$\begin{aligned} P_{\mathcal{S}} = |\mathcal{S}|^{-1}\sum_{g\epsilon\mathcal{S}} g &= 2^{-|\mathcal{G}|}\sum_{a_1,a_2,...\epsilon\{0,1\}}\left(\prod_{g_i\epsilon\mathcal{G}}(g_i)^{a_i}\right) \\ &= \prod_{g_i\epsilon\mathcal{G}}\left(\frac{1}{2}(I+g_i)\right) = \prod_{g\epsilon\mathcal{G}} P_g \end{aligned} \tag{2.4}$$

where $P_g = \frac{1}{2}(1+g)$ is the projector onto the +1 eigenspace of g. This again emphasizes the idea that all of the properties of $\mathcal{S}$ are contained directly in $\mathcal{G}$.

We can now describe the primary advantage of the stabilizer formalism. When $|\mathcal{G}| = N$, the stabilized subspace is one-dimensional i.e., the generators specify a single state (up to an overall phase). This state is called the *codeword* of the stabilizer group. This will be the state of our quantum system. This state can be described by N generators, and each generator $g = (i)^{b_1}(-1)^{b_2}X_1^{a_1}Z_1^{a_2}X_2^{a_3}Z_2^{a_4}...$ can be described by $2N+2$ bits a_i, b_i. The overall factor of $i^{b_1}(-1)^{b_2}$ will be unimportant, as it does not affect the entanglement properties of the state, and will be ignored for the remainder of the chapter. This will be demonstrated in

Sec. 2.6.1, where we will see that the formula for bipartite entanglement entropy is related to the Pauli matrices that make a stabilizer, but is not related to the overall factor. Thus, we can describe the state using $2N^2$ bits. This is a drastic simplification from the canonical description of a state as a vector in the Hilbert space, which in general requires 2^N complex numbers.

2.1.2 Measurement

Another important property of the stabilizer formalism is that it allows us to perform projective measurements. Projections of the state onto single-site Pauli eigenstates can be described entirely in the stabilizer formalism. Therefore we can use the formalism to study dynamics which include such projective measurements.

To be concrete, let $|\psi\rangle$ be a codeword described by the generating set $\mathcal{G}$, and let a projective measurement be applied to the state which collapses it into an eigenstate of Z_x, the Pauli Z operator at site x. The projector for this measurement is given by $P_s = \frac{1}{2}(1+sZ_x)$, where $s = \pm 1$ is the eigenvalue after projection. Z_x is a Pauli matrix at site x, and thus a Pauli string acting as the identity at all other sites. This means Z_x must either commute or anticommute with the generators of $|\psi\rangle$. Rearrange the elements of $\mathcal{G}$ such that all elements g_j, $j < l$ commute with Z_x, and those with $j \geq l$ anticommute with Z_x. Note that at this point, if $|\psi\rangle$ is already a Z_x eigenstate, $\pm Z_x \in \mathcal{S}$, and thus all of the generators commute with it. Then measurement will be trivial, since the state does not change, and the outcome is determined by the Z_x eigenvalue of $|\psi\rangle$. Otherwise, we need to change the set $\mathcal{G}$ while keeping it a generating set of $\mathcal{S}$. In particular, if two generators g_j and g_k anticommute with Z_x, we can replace one with their product $g_j g_k$, which commutes with Z_x. Since the generators are independent, this results in another generating set for the same stabilizer group, but with one less generator that anticommutes with Z_x. If we continue this for the remaining anticommuting generators, we will be left with a generating set where only one generator does not commute with Z_x. We'll call this anticommuting generator g^*.

Consider the commuting generators, $g \neq g^*$, as elements of their own generating set $\mathcal{G}^*$.

These $n-1$ generators stabilize a two-dimensional subspace. Our original codeword, $|\psi\rangle$, lives in the $g^* = +1$ eigenspace of this stabilized subspace. If we now apply the projector P_s to our state, the generators of $\mathcal{G}^*$ will still be stabilizers of our state, as they commute with Z_x and therefore also commute with P_s:

$$gP_s|\psi\rangle = P_s(g|\psi\rangle) = +(P_s|\psi\rangle).$$

Thus the state after projection will be stabilized by $\mathcal{G}^*$ and sZ_x. All of these elements are independent and mutually commute, and thus form a generating set which we will call $\mathcal{G}'$. Since $|\mathcal{G}'| = N$, there is a unique codeword stabilized by the stabilizer group generated by $\mathcal{G}'$, and the above shows that every element in $\mathcal{G}'$ stabilizes $P_s|\psi\rangle$. Thus $\mathcal{G}'$ stabilizes the state which results from a Z_x measurement.

Therefore, we can compute the result of a measurement by staying in the stabilizer formalism. This is done by modifying the generating set to only have one noncommuting generator, and then replacing that generator with $\pm Z_x$. In our simulation, however, we do not keep track of the overall sign. This forces the state into one particular measurement outcome, instead of randomly choosing between the possible outcomes. This does not have major consequences for our results, because the Born probability is equal for both possible outcomes:

$$P(Z_x = +1) = |\langle\psi|P_+|\psi\rangle|^2 = \left|\langle\psi|\tfrac{1}{2}(1+Z_x)g^*|\psi\rangle\right|^2 = \left|\langle\psi|g^*\tfrac{1}{2}(1-Z_x)|\psi\rangle\right|^2 = P(Z_x = -1).$$

Thus, both outcomes will contribute equally to the average over all possible circuit realizations. Since the observables that are calculated at the end of the simulation are insensitive to the overall signs of the generators, we can safely ignore this sign.

2.1.3 Clifford Operations

The Clifford group is defined as the group of all unitary operators that preserve the Pauli group under conjugation i.e., for all Pauli strings $g \in \mathcal{P}_N^2$, a Clifford unitary operator U satisfies $UgU^\dagger \in \mathcal{P}_N^2$. We define $\mathcal{C}_N$ to be this set of operators on N qubits (modulo the overall

$U(1)$ phase factor for each U, which always cancels under conjugation). The most relevant property of this group is that applying a Clifford operation to a codeword returns another codeword, and therefore the result can be described by a group of stabilizers. Further, we can easily calculate the generating set of this new codeword. Since $g \in \mathcal{G}$ is a stabilizer of the state $|\psi\rangle$, $(UgU^\dagger)(U|\psi\rangle) = +U|\psi\rangle$. Thus, the elements of $U\mathcal{G}U^\dagger = \{UgU^\dagger | g \in \mathcal{G}\}$ stabilize the state $U|\psi\rangle$. Since the Clifford group induces a group isomorphism under conjugation, all of the elements of $U\mathcal{G}U^\dagger$ are independent, and thus still form a valid generating set for the codeword.

The canonical matrix form of Clifford operators (i.e., complex $2^N \times 2^N$ matrices) is not well suited to our approach. Instead, we represent the operators by their action on Pauli strings. This associates each Clifford operation to a matrix of integers, and automatically ignores the overall $U(1)$ factor. We will give a formal introduction to this representation in Sec. 2.3.

2.2 Quantum d-level Systems

We now introduce the generalization of the above to systems of qudits, following the work of Refs. [14, 15]. Each site now hosts a d-dimensional local Hilbert space, where d is taken to be a prime number. The *generalized Pauli matrices* now have d eigenvalues which are the d-roots of unity. We denote these eigenvalues by ω such that $\omega^d = 1$.

We now describe this formalism by giving the following list of major differences between the qubit and qudit cases.

- We define the generalized Pauli matrices Z and X by the following actions on the d-level system: $Z|k\rangle = \omega^k |k\rangle$, and $X|k\rangle = |k+1 \bmod d\rangle$. These are often also called the *clock* and *shift* matrices. We define $Y = Z^\dagger X^\dagger$. All generalized Pauli matrices are unitary, but not hermitian.

– As an example, for $d = 3$,

$$X = \begin{pmatrix} 0 & 0 & 1 \\ 1 & 0 & 0 \\ 0 & 1 & 0 \end{pmatrix} \qquad Y = \begin{pmatrix} 0 & 1 & 0 \\ 0 & 0 & \omega^2 \\ \omega & 0 & 0 \end{pmatrix} \qquad Z = \begin{pmatrix} 1 & 0 & 0 \\ 0 & \omega & 0 \\ 0 & 0 & \omega^2 \end{pmatrix} \tag{2.5}$$

- The *generalized commutation relations* are

$$ZX = \omega XZ \qquad XY = \omega YX \qquad YZ = \omega ZY \tag{2.6}$$

The cyclicity in this definition between X, Y, and Z motivates the above definition of Y.

- The *generalized Pauli group* $\mathcal{P}_N^d$ is the group of all generalized Pauli strings, each of which is the tensor product over all sites of the system where the factors are products of generalized Pauli matrices and the identity at each site. In general, two Pauli strings will have a commutation relation of the form $gh = \omega^m hg$ for some $m \in \mathbb{Z}_d$.

- For a system with N sites, the Hilbert space is d^N dimensional. Many of the previous proofs continue to hold, with the on-site dimension 2 replaced by d.

  – A stabilizer group is a commuting subgroup $\mathcal{S}$ of $\mathcal{P}_N^d$.

  – The operator

$$P_{\mathcal{S}} = |\mathcal{S}|^{-1} \sum_{g \in \mathcal{S}} g \tag{2.7}$$

  is a projector onto the stabilized subspace $V_{\mathcal{S}}$ of states with $g|\psi\rangle = +|\psi\rangle$ for all $g \in \mathcal{S}$. This justifies the name stabilizer group.

  – A generating set $\mathcal{G} \subset \mathcal{S}$ contains generators from which we can produce all elements in the stabilizer group through multiplication. If the generators are independent, then any element $g \in \mathcal{S}$ can be written as a unique product $g = g_1^{a_1} g_2^{a_2} \ldots$ for generators $g_j \in \mathcal{G}$ and exponents $a_j \in \mathbb{Z}_d$. This shows that $|\mathcal{S}| = d^{|\mathcal{G}|}$.

– We can write the projector $P_{\mathcal{S}}$ in terms of elements of a generating set,

$$P_{\mathcal{S}} = \prod_{g \in \mathcal{G}} P_g, \tag{2.8}$$

where $P_g = d^{-1} \sum_{k=0}^{d-1} g^k$ is the projector onto the +1 eigenspace of the generator g.

– Taking the trace of $P_{\mathcal{S}}$ gives the result $dim(V_{\mathcal{S}}) = d^{N-|\mathcal{G}|}$. This means that we can still represent a codeword with N generators or $2N^2$ integers. However, those integers will be taken from $\mathbb{Z}_d$ instead of $\mathbb{Z}_2$.

- Measurements at site x are enacted by the projector

$$P_m = d^{-1} \sum_{k=1}^{d} (\omega^m)^{-k} (Z_x)^k \tag{2.9}$$

which projects the state into a $Z_x = \omega^m$ eigenstate.

- The process for taking a Z_x measurement has the same form. The state is first represented through a generating set. Then this set is modified into a new generating set that generates the same stabilizer group, and that has only a single generator that does not commute with Z_x. The final noncommuting generator is then replaced by Z_x.

  However, generators can have any multiple of ω as a phase when commuting past the operator Z_x. We still multiply elements together to make commuting generators, but we may need to multiply powers of generators together in order to force the product to commute. This is the primary reason that we require d to be prime. Replacing a generator with a power of itself, $g_i \mapsto (g_i)^k$, does not need to result in a generating set which generates the same stabilizer group if k divides d. For example, if $d = 6$ then g^2 can be generated from powers of g, but g cannot be generated from powers of g^2, and thus replacing g with g^2 will result in a generating set which does not generate the same stabilizer group. This cannot happen for prime d, and thus taking powers of generators is always a valid replacement.

- The Clifford group $\mathcal{C}_N$ is now defined to be the group of unitary operators which map generalized Pauli strings to generalized Pauli strings under conjugation: $U\mathcal{P}_N^d U^\dagger = \mathcal{P}_N^d$. For a codeword $|\psi\rangle$ which is described by the generating set $\mathcal{G}$ of generalized Pauli strings, the codeword $U|\psi\rangle$ is described by the generating set $U\mathcal{G}U^\dagger$.

2.3 State and Operator Representations

We now turn to describe how the state will be represented using the stabilizer formalism. It was previously mentioned that the system will be described by a $N \times 2N$ matrix if integers modulo d. We now describe this in detail, and explain how this matrix updates when acted on by our dynamics.

There are two operations which are applied to the system. We alternately apply a random two-qudit Clifford operation to each pair of neighboring sites and then take a projective Z_x measurement with probability p for every site x. We will first introduce a concrete notation for representing our state in an efficient way. We will then introduce the corresponding representation of Clifford operations. The following formalism will apply to qudits of prime order d.

For a Pauli string g, we write $\vec{r}(g)$ to represent the row vector of $2N$ integers mod d which describe the string in terms of its exponents. Specifically, if $g = X_1^{a_1} Z_1^{a_2} X_2^{a_3} Z_2^{a_4} ...$, then $\vec{r}(g) = (a_1,\ a_2,\ a_3, ...) \in (\mathbb{Z}_d)^{2N}$. Note that this is different from the more common representation which groups together the exponents from the X and Z operators. We again mention that we are explicitly ignoring the overall phase of the generator, as it will have no impact on the quantities that will be calculated. A set of N independent generators will uniquely identify a codeword (up to an overall phase), and thus the state will be represented by a $N \times 2N$ matrix called the *check matrix* in which each row corresponds to a generator.

We note that multiplication of Pauli strings corresponds to the addition of row vectors (up to an overall phase):

$$\vec{r}\left(X^{a_1} Z^{a_2} X^{b_1} Z^{b_2}\right) = \vec{r}\left(\omega^{a_2+b_1} X^{a_1+b_1} Z^{a_2+b_2}\right) = (a_1 + b_1,\ a_2 + b_2) = \vec{r}\left(X^{a_1} Z^{a_2}\right) + \vec{r}\left(X^{b_1} Z^{b_2}\right)$$

As a result, the generators of our codeword are independent if and only if the rows of the check matrix are linearly independent. In addition, Clifford operations can be represented as matrices acting on $\vec{r}(g)$. Clifford conjugation implies linearity for its action on $\vec{r}(g)$:

$$U(gh)U^\dagger = (UgU^\dagger)(UhU^\dagger) \qquad \Longrightarrow \qquad \vec{r}(gh)C_U = \vec{r}(g)C_U + \vec{r}(h)C_U$$

where C_U is the matrix representing the action of conjugation by U.

However, not all matrices represent the action of a Clifford operator. First, the matrices must be invertible modulo d, since the Clifford operators are invertible. Second, they must preserve the commutation relations between any Pauli strings:

$$(UgU^\dagger)(UhU^\dagger) = UghU^\dagger = \omega^k UhgU^\dagger = \omega^k (UhU^\dagger)(UgU^\dagger).$$

This leads us to consider a method for finding the commutation relation of any two Pauli strings using only their row representation. This can be done by introducing an inner product on the vector space $(\mathbb{Z}_d)^{2N}$, which we denote $\langle \cdot, \cdot \rangle$. This inner product will encode the commutation relations of the operators by giving the exponent of ω:

$$gh = \omega^{\langle \vec{r}(g), \vec{r}(h) \rangle} hg$$

The algebra of the Pauli strings allows a consistent definition of this inner product, and requires it to have the following two properties:

$$\begin{aligned} &\textit{linearity:} && \langle \vec{u}, \vec{v} + \vec{w} \rangle = \langle \vec{u}, \vec{v} \rangle + \langle \vec{u}, \vec{w} \rangle \\ &\textit{antisymmetry:} && \langle \vec{v}, \vec{w} \rangle = -\langle \vec{w}, \vec{v} \rangle \end{aligned}$$

An inner product which satisfies these properties is called a *symplectic* inner product[1]. These properties imply that there exists a *symplectic metric* Ω such that

$$\Omega^\top = -\Omega$$

$$\langle \vec{v}, \vec{w} \rangle = \vec{v} \Omega \vec{w}^\top$$

[1]The definition of a symplectic form $\langle \cdot, \cdot \rangle$ also requires that it be *nondegenerate*. However, we have an explicit form of the symplectic metric Ω which is invertible, and this implies that the inner product will be nondegenerate.

This allows us to state our constraint on valid Clifford actions, C_U. Conjugation by a Clifford operator U does not change the commutation relations. Therefore,

$$\langle \vec{v}C_U, \vec{w}C_U \rangle = \langle \vec{v}, \vec{w} \rangle \qquad \Longrightarrow \qquad C_U \Omega C_U^\top = \Omega \tag{2.10}$$

This is the defining property that C_U be a *symplectic matrix*. Therefore, to find a random Clifford action on our system, we must find a random symplectic matrix on this vector space.

There is a subtlety here. By writing the action of a Clifford operator in this way, we only retain information about how the Pauli operators are mapped to each other. We also need some data about the phases if we want to uniquely determine the Clifford action. For instance, when $d = 2$ the two mappings

$$\begin{cases} X \mapsto -Y = iXZ \\ Z \mapsto Z \end{cases} \qquad \text{and} \qquad \begin{cases} X \mapsto Y = -iXZ \\ Z \mapsto -Z \end{cases}$$

are both automorphisms of $\mathcal{P}_1^2$. In the row representation they both have the action $X \mapsto XZ$, and $Z \mapsto Z$. These phases do not affect the values of the quantities that will be measured, so they can be ignored. But it must still be shown that this does not affect the uniformity of our sampling i.e., whether choosing a symplectic matrix with a uniform distribution will correspond to choosing a Clifford operator with a uniform distribution.

With some thought it can be seen that all such mappings are enacted by a single Clifford operator multiplied by different Pauli strings (which are themselves Clifford operators). For instance, in the above example

$$\begin{aligned} UXU^\dagger = iXZ \qquad &\Longrightarrow \qquad (UY)X(UY)^\dagger = -iXZ \\ UZU^\dagger = Z \qquad &\Longrightarrow \qquad (UY)Z(UY)^\dagger = -Z \end{aligned}$$

Therefore, each valid symplectic mapping C_U represents a class of Clifford operators which are related to each other by the multiplying of Pauli strings [29]. In particular, all such classes are of the same size. Thus choosing a random symplectic matrix will correspond to a uniform distribution over Clifford operators.

2.4 Picking Symplectic Matrices

The symplectic group $Sp(\mathbb{Z}_d, 2n)$ is the group of all $2n \times 2n$ matrices with coefficients in $\mathbb{Z}_d$. Clifford operations are represented by elements of this group. In order to generate a random two-qudit Clifford action, we must find a method for picking a random element of $Sp(\mathbb{Z}_d, 4)$, a 4×4 symplectic matrix corresponding to a random two-site Clifford unitary gate.

The following method for picking a random symplectic matrix is adapted from Ref. [29]. The core idea is that a random $2n \times 2n$ symplectic matrix can be created by picking a random symplectic basis for the abstract vector space $(\mathbb{Z}_d)^{2n}$. We do this by using a modified version of Gram-Schmidt orthonormalization.

2.4.1 Gram-Schmidt Process

Start with a set of vectors $\mathcal{Q} \subset (\mathbb{Z}_d)^{2n}$. The set can be of any size, and the vectors can be linearly dependent. We choose one vector v from the set, then search $\mathcal{Q}$ to find any vector which is conjugate to it i.e., a $w \in \mathcal{Q}$ such that $\langle v, w \rangle = 1$. As long as there is at least one vector y such that $\langle v, y \rangle = k$, then we can choose $w = k^{-1}y$. The inverse k^{-1} is always defined when d is prime. Then, other vectors in $\mathcal{Q}$ are mapped to a new set $\mathcal{Q}'$ via

$$f \mapsto f' = f - \langle v, f \rangle w + \langle w, f \rangle v. \tag{2.11}$$

These will all be orthogonal (in the symplectic sense) to both v and w, since

$$\begin{aligned}
\langle v, f' \rangle &= \langle v, f \rangle - \langle v, f \rangle \langle v, w \rangle + \langle w, f \rangle \langle v, v \rangle \\
&= \langle v, f \rangle - \langle v, f \rangle (1) + (0) = 0, \\
\langle w, f' \rangle &= \langle w, f \rangle - \langle v, f \rangle \langle w, w \rangle + \langle w, f \rangle \langle w, v \rangle \\
&= \langle w, f \rangle - (0) + \langle w, f \rangle (-1) = 0.
\end{aligned}$$

Note that after this mapping, a vector f' which is orthogonal to both v and w must be linearly independent of both w and v. This is because w is now the only vector in $\mathcal{Q}'$ such that $\langle v, w \rangle \neq 0$. Therefore if a vector f' has any nonzero w component it cannot have

$\langle v, f' \rangle = 0$. The same follows for v. Thus, all elements f' must lie in a vector subspace perpendicular to the span of v and w.

We now have a symplectic pair, (v, w), and an independent set of vectors $\mathcal{Q}'$ such that $\mathcal{Q}$ and $\mathcal{Q}' \cup \{v, w\}$ span the same vector space. If we want a symplectic basis for the entire space, then we repeat this process on $\mathcal{Q}'$ until we have enough independent symplectic pairs to span the vector space.

2.4.2 Random $\mathbb{Z}_d$ Symplectic

Now, we can pick a random symplectic matrix from the group $Sp(\mathbb{Z}_d, 4)$, which corresponds to a two-qudit Clifford operator. This is based on the process described in [29]. We essentially form a random symplectic basis for the vector space $(\mathbb{Z}_d)^4$, and these become the columns of our matrix.

We start with the most basic basis for the space, which we arrange as the identity matrix i.e., $e_1 = (1, 0, 0, 0)$, $e_2 = (0, 1, 0, 0)$, etc. This forms our set $\mathcal{Q}$, with 4 elements. Next, choose a random nonzero vector $v_1 \in (\mathbb{Z}_d)^4$. Then, search through $\mathcal{Q}$ for a conjugate vector, and call it $\tilde{f}$. If we find any vector f with a nonzero symplectic product, we can pick $\tilde{f} = \langle f, v_1 \rangle^{-1} f$. We use $\tilde{f}$ to project the other vectors in $\mathcal{Q}$ onto the subspace orthogonal to v_1 via the mapping

$$f_i \mapsto f_i' = f_i - \langle v_1, f_i \rangle \tilde{f}.$$

Now that we have picked a symplectic partner $\tilde{f}$ of v_1, we need to turn this into a *random* symplectic partner w_1 of v_1, chosen from a uniform distribution over all possible symplectic partners. Fortunately, our set of vectors f_i' gives us an easy way to do this. Because of the linearity of the symplectic product, all vectors which are symplectic partners of v_1 will differ from each other by vectors which are orthogonal to v_1. Our vectors f_i' form a basis which spans the three-dimensional subspace of $(\mathbb{Z}_d)^4$ which is orthogonal to v_1, and thus give a way to describe each possible symplectic pair w_1. To prove this, assume the opposite: there are coefficients c_i such that $\sum c_i f_i' = 0$. Then,

$$0 = \sum_{i=1}^{3} c_i f_i' = \sum_{i=1}^{3} c_i f_i - \left(\sum_{i=1}^{3} c_i \langle v_1, f_i \rangle \right) \tilde{f}$$

However, the vectors $\{f_i, \tilde{f}\}$ originally formed a basis, and so form an independent set. The above is a linear superposition of independent vectors, and thus the equation can only be satisfied if every $c_i \equiv 0 \mod d$. We can thus get a random symplectic partner by choosing a random orthogonal vector from this subspace and adding it to our chosen symplectic partner $\tilde{f}$.

We use this to get a random symplectic partner w_1, and use v_1 and w_1 to orthogonalize the remaining subspace via the Gram-Schmidt process described in Eq. 2.11. The images of the three remaining vectors will be linearly dependent, since they span the two-dimensional subspace orthogonal to both v_1 and w_1. We then perform the modified Gram-Schmidt orthogonalization process on these three vectors to get a symplectic matrix.

Note that one of the vectors will be discarded in the final step. At some point in the process, one vector will become orthogonal to all the other vectors in the set. Since the set spans our vector space, this can only happen if that vector is equal to zero.

This process does not randomize the final two vectors but only orthogonalizes them. Thus this process gives us a random sampling of the mapping of the first two Pauli operators, which correspond to the operators of the first qudit. To find a fully random symplectic matrix, we will now find a random 2×2 symplectic matrix C_2 and multiply the previous 4×4 result with $I \oplus C_2$. This results in a completely random 4×4 symplectic matrix, as demonstrated using the following proof [29]. For a finite group G with a nested chain of subgroups

$$G_1 \subset G_2 \subset ... \subset G_{n-1} \subset G_n = G$$

we can make a map from the cosets to the group via

$$(G_n/G_{n-1}) \times (G_{n-1}/G_{n-2}) \times ... \times (G_2/G_1) \times G_1 \mapsto G$$
$$([g_n], [g_{n-1}], ..., [g_2], g_1) \mapsto g_n \cdot g_{n-1} \cdot ... \cdot g_2 \cdot g_1.$$

This map is an isomorphism. If we write the elements of $Sp(\mathbb{Z}_d, 2)$ as $I \oplus C_2$, we can see that these are a subgroup of $Sp(\mathbb{Z}_4, 4)$ which act as the identity for a certain two-dimensional subspace. We will take this subspace to be the first two vectors acted on by the matrix. Thus

a coset in $Sp(\mathbb{Z}_d, 4)/Sp(\mathbb{Z}_4, 2)$ is represented by a matrix of the form we have constructed: a matrix corresponding to a symplectic basis with a particular choice for only the first two vectors. The result immediately follows. By using our process to find a representative of the class $Sp(\mathbb{Z}_d, 4)/Sp(\mathbb{Z}_4, 2)$, we can uniformly sample all of $Sp(\mathbb{Z}_d, 4)$ by finding a random element $I \oplus C_2 \in Sp(\mathbb{Z}_d, 2)$ and multiplying it with our representative.

For $d = 2$, there are 6 possible 2×2 symplectic matrices, so it is easy to find them explicitly. For higher levels, we repeat the above algorithm using two-component vectors to get a random 2×2 symplectic matrix.

2.5 The Clipped Gauge

Now, we focus on the process of extracting information from our system. In particular, there are three quantities which we focus on. For pure states, these are the bipartite subsystem entanglement entropy and the normalized stabilizer length distribution. The latter quantity is intimately related to the entanglement entropy, as we will show in Sec. 2.6.3. For mixed states, this is the total entropy (or purity), which is a measure of the statistical entropy of the mixed state. In order to calculate these quantities, we first manipulate the generating set so that it conforms to a set of constraints. This places the generating set in what is known as the *clipped gauge* [30] which gives an unambiguous way of extracting these quantities.

Given a stabilizer group $\mathcal{S}$, the choice of a minimal generating set $\mathcal{G}$ is not unique. It is helpful to view this ambiguity as a type of gauge invariance, and choosing a specific $\mathcal{G}$ is akin to choosing a gauge. In this language, the clipped gauge is a gauge-fixing condition which, in some sense, forces each of our generators to act on the smallest region possible. There is still some gauge freedom, even given the clipped gauge condition; but any generating set which is in the clipped gauge will have the same number of stabilizers acting in the same region. This gives us an unambiguous way to study the average length of the stabilizers in the stabilizer group, which is a way of quantifying how entangled the system is. It also simplifies the process of finding all stabilizers which act only in some region A, which form the group $\mathcal{S}_A \subset \mathcal{S}$, and is crucial to calculating the subsystem entropy.

We define the clipped gauge as follows. We first define the function $\rho_l(x)$ to be the number of stabilizers which have their leftmost nontrivial action at site x of our system. $\rho_r(x)$ is defined similarly, but for the rightmost nontrivial action. With this, the clipped gauge condition is [30, 1]:

1. For all sites x in the system, $\rho_l(x) + \rho_r(x) \leq 2$.

2. For any site x, if $\rho_l(x) = 2$ or $\rho_r(x) = 2$, then the action of the two generators which have their left (right) endpoint at x have a different action at the site x.

The clipped gauge is possible with d-level systems. We show this by giving the algorithm which places a generating set into the clipped gauge for d-level systems. The centerpiece of this algorithm involves a modified matrix row reduction, where we replace rows with linear combinations of other rows in the matrix. In terms of operators, this is equivalent to replacing a generator in the set with a product of other generators. The algorithm is as follows:

- First represent the generating set in the form of an $N \times 2N$ check matrix. Each row $\vec{r}(g)$ represents a generator g, and each entry corresponds to the exponent of an X or Z operator in a Pauli string.

- Perform row reduction on this matrix, focusing on the left endpoints.

  - By adding rows to each other, we are creating a different generating set where one generator is replaced by the product of other generators. Since the generators are independent, the rows are linearly independent; and since row reduction does not change the span of the row vectors, our new generating set will generate the same stabilizer group.

  - After row reduction, there cannot be more than one leftmost nonzero entry per column. There may be two nonzero entries for a pair of columns that represent

a single qudit e.g., $(1\,0) \sim X$ and $(0\,2) \sim Z^2$, but their actions at this site must be independent. This satisfies the second condition of the clipped gauge for left endpoints, and also implies $\rho_l(x) \leq 2$.

- Do row reduction again, focusing on the right endpoints. Start cancelling rightmost entries by adding multiples of the row whose left endpoint is farthest to the right, so that the left endpoints will not be changed. Continue until there is only one right endpoint per column. Again we can have two operators on one site, but they must act independently, so $\rho_r(x) \leq 2$.

It is clear from the above that the resulting matrix will satisfy the second property of the clipped gauge. To show that it satisfies the first property, we must show that there are not three or more endpoints at any one site. This follows from the requirement that all stabilizers in the generating set must commute with each other. For if we had three endpoints at a site x e.g., two left endpoints and one right endpoint, then the generator with its right endpoint at x only overlaps the other two generators at site x. Thus, its action at x must commute with the action of the other two generators at x in order for the generators to mutually commute. However, the other two generators have actions at x which are independent of each other, as shown above, and it is impossible for any operator in the Hilbert space of x to commute with them both. This is a contradiction, and the conclusion is that we cannot have a site with two left endpoints and a right endpoint; $\rho_l(x) + \rho_r(x) \leq 2$. For pure states, Since there are N sites and $2N$ endpoints, $\rho_l(x) + \rho_r(x) = 2$ for all sites; however, for mixed states we will generally have the inequality.

2.6 Entropy and Length Distribution

We now describe the equations used to calculate two significant quantities which result from our calculations: the subsystem entanglement entropy and normalized stabilizer length distribution.

2.6.1 Entropy from stabilizers

To characterize the entanglement entropy, we will use a *bipartite subsystem entanglement entropy*. We first choose a subsystem of sites A, and denote as $\bar{A}$ the subsystem's complement which contains every site not in A. In the next section, we will specialize to contiguous subsystems. However, the results of this section do not require A to be contiguous.

A convenient measure of bipartite entropy to use for stabilizer states is given by the Rényi entropies. The n^{th} Rényi entropy, for $n > 1$, is defined as

$$S_n(A) = \frac{1}{1-n}\log_d \operatorname{Tr}({\rho_A}^n) \tag{2.12}$$

Note that we are defining these entropies with a base d logarithm. $\rho_A = \operatorname{Tr}_{\bar{A}}\rho$ is the reduced density matrix for subsystem A, given by a partial trace over the complement $\bar{A}$, which we will now describe. Schematically, we can write our density matrix as

$$\rho = |\psi\rangle\langle\psi| = \sum_{jklm} C_{jk}C^*_{lm}\,|j_A k_{\bar{A}}\rangle\langle l_A m_{\bar{A}}| \tag{2.13}$$

where $|j_A\rangle$ is a set of basis states on A and $|k_{\bar{A}}\rangle$ is a set of basis states on $\bar{A}$. The partial trace over $\bar{A}$ is given by

$$\rho_A = \operatorname{Tr}_{\bar{A}}(\rho) = \sum_{jlr} C_{jr}C^*_{lr}\,|j_A\rangle\langle l_A|\,.$$

This density matrix generally represents a mixed state over the subsystem A.

It's worth noting that the Rényi entropy becomes the von Neumann entropy in the limit $n \to 1$, where the von Neumann entropy is defined by

$$S = -\operatorname{Tr}(\rho_A \log \rho_A).$$

The von Neumann entropy is a direct quantum generalization of the Shannon entropy from information theory. For a stabilizer codeword, we will show that the Rényi entropies are the same for all values of n, and thus equal to the von Neumann entropy.

The Rényi entropy is convenient, because it can be calculated directly from the generating set of our stabilizer group. We give a derivation of this, following Appendix C in Ref. [30],

but generalized to qudits. As shown following Eq. (2.2), the sum of all elements in the stabilizer group is a projector onto the stabilized codeword:

$$P_{\mathcal{S}} = |\mathcal{S}|^{-1} \sum_{g \in \mathcal{S}} g = d^{-N} \sum_{g \in \mathcal{S}} g$$

For a pure state, $\rho = |\psi\rangle\langle\psi|$ is a projector onto $|\psi\rangle$, from which it follows $\rho \propto P_{\mathcal{S}}$. We can find the overall factor by comparing the trace of $P_{\mathcal{S}}$ to $\mathrm{Tr}(\rho) = 1$. However, the trace of a projector is equal to the dimension of the subspace that it projects onto, and $P_{\mathcal{S}}$ projects onto a one-dimensional codeword. Thus, $\mathrm{Tr}(P_{\mathcal{S}}) = 1$, and we conclude that $\rho = P_{\mathcal{S}}$.

If we now split the system into two parts, A and $\bar{A}$, we have

$$\rho_A = \mathrm{Tr}_{\bar{A}} \rho = d^{-N} \sum_{g \in \mathcal{S}} \mathrm{Tr}_{\bar{A}}(g)$$

However, any element g in $\mathcal{S}$ is a tensor product of generalized Pauli matrices at each site. An important property of the partial trace it that it, like the full trace, has following factoring property:

$$\mathrm{Tr}_A(Q \otimes R) = \mathrm{Tr}_A(Q) \cdot \mathrm{Tr}_A(R). \tag{2.14}$$

Using this and the fact that $\mathrm{Tr}(X) = \mathrm{Tr}(Y) = \mathrm{Tr}(Z) = 0$, we see that $\mathrm{Tr}_{\bar{A}}(g)$ will vanish unless it acts as the identity on $\bar{A}$. If so, $\mathrm{Tr}(I) = d$ implies that the value of the partial trace over these identities will be $d^{|\bar{A}|}$, leading to

$$\rho_A = d^{-N} d^{|\bar{A}|} \sum_{g \in \mathcal{S}_A} g|_A = d^{-|A|} \sum_{g \in \mathcal{S}_A} g|_A,$$

where $\mathcal{S}_A$ is the subgroup of elements in $\mathcal{S}$ which act trivially on $\bar{A}$, and the operators $g|_A$ are the restriction of the elements g to the subsystem A.

We can create a generating set $\mathcal{G}_A$ for $\mathcal{S}_A$. It is important to note that in general, $\mathcal{G}_A \notin \mathcal{G}$; that is, given a generating set $\mathcal{G}$ we cannot in general expect $\mathcal{G}_A$ to simply be the set of elements in $\mathcal{G}$ which act trivially on $\bar{A}$. This is because there might be combinations of the generators in $\mathcal{G}$ which act trivially on $\bar{A}$ even though they themselves do not. Applying Eq. (2.2) to $\mathcal{S}_A$, we can rewrite ρ_A as

$$\rho_A = d^{-|A|} |\mathcal{S}_A| \left[|\mathcal{S}_A|^{-1} \sum_{g \in \mathcal{S}_A} g|_A \right] = d^{-|A|} |\mathcal{S}_A| P_{\mathcal{S}_A}$$

Since $P_{\mathcal{S}_A}$ is a projector, $(P_{\mathcal{S}_A})^2 = P_{\mathcal{S}_A}$, and

$$\rho_A{}^2 = d^{-|A|}|\mathcal{S}_A|\rho_A = d^{|\mathcal{G}_A|-|A|}\rho_A. \tag{2.15}$$

Thus, for any value of n, the Rényi entropy is

$$\begin{aligned} S_n(A) &= \frac{1}{1-n}\log_d \mathrm{Tr}((\rho_A)^n) \\ &= \frac{1}{1-n}\log_d \left\{(d^{|\mathcal{G}_A|-|A|})^{n-1}\mathrm{Tr}\rho_A\right\} \\ &= -\log_d \left\{d^{|\mathcal{G}_A|-|A|}\right\} = |A| - |\mathcal{G}_A|. \end{aligned} \tag{2.16}$$

Therefore, if we have an efficient way of deciding the size of the generating set $\mathcal{G}_A$, it will immediately give us the subsystem entropy of A.

2.6.2 Calculating Entropy in the Clipped Gauge

We will now give the details of using the clipped gauge to calculate the subsystem entropy. We show that in the clipped gauge, all of the necessary data to calculate the bipartite subsystem entanglement entropy for contiguous subsystems A_i will be contained in the locations of the endpoints of the generators. We first show that for *contiguous* subsystems A of the state, the generating set $\mathcal{G}_A$ is the set of generators (in the clipped gauge) that are supported entirely within the subsystem. From this we will deduce that the subsystem entanglement entropy can be calculated entirely from the number of generators that have one endpoint in each of the subsystems A and $\bar{A}$, and thus $S_n(A)$ can be calculated from the locations of the endpoints of the generators in the clipped gauge.

We first look at the subsystem entanglement entropy for *properly contiguous* subsystems. For a system with sites labelled $1, 2, ..., N$, a properly contiguous subsystem of length L is defined to be a subsystem containing all sites $j, j+1, ..., j+L-1$, where the rightmost endpoint $(j+L-1) \leq N$. Since we are considering periodic boundary conditions, we should also consider the subsystem entropy of "periodic-contiguous" subsystems consisting of sites $j, ..., N, 1, 2...$, as well. However, a property of any bipartite entanglement entropy is that

the entropy $S(A)$ is the same as the entropy of its complement $S(\bar{A})$. So we can calculate the entropy of this periodic-contiguous subsystem by finding the entropy of its properly contiguous complement.

The entropy of a region A is determined by the subgroup $\mathcal{S}_A$ of stabilizers supported on A, which clearly doesn't depend on the choice of generators $\mathcal{G}_A$ we use to define it. However, for a generating set $\mathcal{G}$ of $\mathcal{S}$, it's not generally true that $\mathcal{G}_A \subset \mathcal{G}$. In particular, there may be some combination of $g_1^{a_1} g_2^{a_2} ...$ of $g_i \in \mathcal{G}$, not all of which are trivial on $\bar{A}$, which nonetheless combine into an element which is trivial on $\bar{A}$, and thus can be used as a generator in $\mathcal{G}_A$.

This is not the case in the clipped gauge for properly contiguous subsystems. Multiplying generators cannot decrease the size of the resulting stabilizer, and therefore elements in $\mathcal{S}_A$ cannot be generated by generators in $\mathcal{G}$ that act outside of A. To be specific, we say that the stabilizer g has *support* A_g if the subsystem A_g is the smallest (properly) contiguous subsystem on which the element g acts nontrivially. The statement that we will now show is that support of a product of clipped gauge generators is the smallest contiguous region which includes the supports of the factors. In particular, a product involving generators which act nontrivially on $\bar{A}$ must itself act nontrivially on $\bar{A}$.

For the following, we assume that the factors being multiplied together are not inverses of each other e.g., $(g)^k$ and $(g)^{d-k}$. Refraining from this, we can otherwise multiply any power of any generator together. To be concrete, focus on the right endpoint of the product of two independent generators (or powers of two generators). If the generators have their endpoints at different sites, then the right endpoint of the product must be the rightmost endpoint of the factors. However, if two independent generators in the clipped gauge share a right endpoint, the two actions at that right endpoint must be independent. Therefore, there is no way that their right endpoints can cancel, and the rightmost endpoint of their product is equal to their shared right endpoint. Furthermore, there can be no more than two endpoints at one site, and so no third generator can exist which cancels the action at that site and reduce the support of the product. The same is true of the left endpoint. Therefore, multiplying independent generators can only increase the size of the support of

their product, and the support of the product must include the supports of all of its factors.

Stabilizers supported within a region A must be the product of generators which are also only supported in A, if those generators are in the clipped gauge. The size of $\mathcal{G}_A$ is given by the number of generators which are supported in the region A. Therefore, for properly contiguous subsystems A, we can easily calculate the subsystem entanglement entropy by counting the number of generators which are supported entirely within A.

We will turn this into a more general equation. Let n_A^{in} be the number of clipped gauge generators which are supported in A, n_A^{out} the number of generators with both endpoints in $\bar{A}$, and $n_A^{\text{cross}} = n_{\bar{A}}^{\text{cross}}$ the number of generators with one endpoint in A and the other in $\bar{A}$. Note that since A is properly contiguous, generators with both endpoints in $\bar{A}$ are generally not supported in $\bar{A}$ since they may cross through A: $n_A^{\text{out}} \neq n_{\bar{A}}^{\text{in}}$. However, what we will show is that we can *effectively* set $n_A^{\text{out}} = n_{\bar{A}}^{\text{in}}$.

Since there are always two endpoints at each site when in the clipped gauge, we have the following relations:

$$2|A| = 2n_A^{\text{in}} + n_A^{\text{cross}}$$
$$2|\bar{A}| = 2n_A^{\text{out}} + n_A^{\text{cross}}$$

Therefore, in the clipped gauge,

$$S_n(A) = |A| - |\mathcal{G}_A| = |A| - n_A^{\text{in}} = n_A^{\text{in}} + \frac{1}{2}n_A^{\text{cross}} - n_A^{\text{in}} = \frac{1}{2}n_A^{\text{cross}} \tag{2.17}$$
$$= n_A^{\text{out}} + \frac{1}{2}n_A^{\text{cross}} - n_A^{\text{out}} = |\bar{A}| - n_A^{\text{out}} \tag{2.18}$$

The first line makes it clear that $S_n(A) = S_n(\bar{A})$, since both have the same number n_A^{cross} of generators with an endpoint in both subsystems. The second line shows us that we can effectively think of n_A^{out} as $n_{\bar{A}}^{\text{in}}$ i.e., for the purposes of calculating subsystem entanglement entropy, we can consider any generator with both endpoints in the system A as being a generator of $\mathcal{G}_A$, as long as that system is contiguous in a system with periodic boundary conditions.

2.6.3 Stabilizer Length Distribution

Another piece of data that we will extract from our systems is the normalized stabilizer length distribution $D_{\mathcal{G}}(L)$, which for a particular system is defined as

$$D_{\mathcal{G}}(L) = \frac{1}{N} \sum_{g \in \mathcal{G}} \delta_{\ell_g, L}, \tag{2.19}$$

where ℓ_g is the length of the support of g. Thus $D_{\mathcal{G}}(L)$ equals the number of generators $g \in \mathcal{G}$ in the clipped gauge that have a support of size L, divided by system size N. Note that this is slightly different than the length distribution introduced in other places, as both endpoints contribute to the length ℓ_g of g (contrast Refs. [1, 4]).

This quantity is well defined in the sense that a stabilizer state will have a unique length distribution, because the support of generators is unique for any generating set which satisfies the clipped gauge. This can most easily be seen through the fact that the positions and lengths of generators can be inferred from the subsystem entanglement entropy. For example, in a two-site subsystem A, $S_n(A) = 2 - |\mathcal{G}_A|$. This allows us to calculate the number of generators supported on A. Further, we can use the entropy of each individual site to calculate the number of generators of length one which are supported on A, and thus infer the number of generators of length two. This generalizes up to subsystems of length L, and allows us to calculate the lengths and locations of all generators by using the entropies $S_n(A)$. Since these entropies are independent of the generating set, it must be that the lengths and locations of the generators are the same for all generating sets in the clipped gauge.

This relationship is reciprocal, as the subsystem-averaged subsystem entanglement entropy $S(L)$ can be calculated from the length distribution, as we now show. First, we define $S(L)$ as the average entropy of all N possible contiguous (with periodic boundary conditions) subsystems A of our system such that the length $|A| = L$:

$$S(L) = \frac{1}{N} \sum_{|A|=L} S_n(A) = \frac{1}{N} \sum_{|A|=L} \frac{1}{2} n_A^{\text{cross}}. \tag{2.20}$$

We only consider regions of length $L \leq N/2$ since $S(L) = S(N-L)$, which follows from the fact that $S_n(A) = S_n(\bar{A})$.

Consider generators g which have a support of length $\ell_g < N/2$. If $\ell_g < L$ then this generator will contribute once to the value of n_A^{cross} for $2\ell_g$ distinct subsystems. If $\ell_g \geq L$, it will contribute to n_A^{cross} for $2(L-1)$ subsystems. If $\ell_g \geq N/2$, we can use the fact that only the locations of the endpoints are considered by n_A^{cross} to effectively think of a generator that is connected in the opposite direction around the periodic boundary of the system. We are then looking at the complement of the support of g as the support of this effective generator, and this has a size of $N - \ell_g$. It will contribute to n_A^{cross} for $2(N-\ell_g)$ subsystems. Thus,

$$S(L) = \frac{1}{N} \sum_{g \in \mathcal{G}} \min(L-1, \ell_g, N-\ell_g) = \sum_{\ell=1}^{N} D_{\mathcal{G}}(\ell) \min(L-1, \ell, N-\ell)$$

Where we used the fact that the number of generators with length ℓ is equal to $N D_{\mathcal{G}}(\ell)$. Thus, the subsystem-averaged subsystem entanglement entropy $S(L)$ can be calculated from the normalized stabilizer length distribution $D_{\mathcal{G}}(L)$.

2.6.4 Purity (Total Entropy)

A mixed state can be described in the stabilizer formalism. It is described as a state with a generating set which is too small to fully define the state. It was shown in Eq. 2.2 and following that the projector

$$P_{\mathcal{S}} = d^{|\mathcal{G}|} \sum_{g \in \mathcal{S}} g = \prod_{g \in \mathcal{G}} P_g$$

projects onto the stabilized subspace $V_{\mathcal{S}}$ of the stabilizer group $\mathcal{S}$, with $\dim(V_{\mathcal{S}}) = \text{Tr}(P_{\mathcal{S}}) = N - |\mathcal{G}|$. See also Eq. 2.7 and Eq. 2.8. For $|\mathcal{G}| = N$, this defines a codeword $|\psi\rangle$, and $P_{\mathcal{S}} = \rho = |\psi\rangle\langle\psi|$ is the density matrix of this pure state.

We now consider a generating set $|\mathcal{G}| < N$, and an operator of the form

$$\rho = d^{-N} \sum_{g \in \mathcal{S}} g = d^{|\mathcal{G}|-N} \prod_{g \in \mathcal{G}} P_g, \qquad \text{Tr}(\rho) = 1.$$

This operator is a valid density matrix, as it is hermitian and has a trace of 1. However, it is not a projector. A calculation following the logic of Eq. 2.3 shows $\rho^2 = d^{|\mathcal{G}|-N}\rho$. Therefore, ρ is a density matrix representing a mixed state.

For a mixed state, one can use the *purity* of the state, defined as

$$\mathrm{Tr}(\rho^2) = e^{-S_2}.$$

This is inversely proportional to the Rényi entropy S_2. However, instead of being a subsystem entanglement entropy, it is the statistical entropy of the entire state. To avoid confusion, we will call this the *total entropy* in this context. When the total entropy is large, the purity is small; when the state is pure and the total entropy is zero, the purity is equal to unity. For a mixed state, this total entropy S_2 (which is identical to S_n for any $n > 1$) is

$$\begin{aligned} S_n = \frac{1}{1-n} \log_d \mathrm{Tr}\left(\rho^n\right) &= \frac{1}{1-n} \log_d \mathrm{Tr}\left(\left(d^{(|\mathcal{G}|-N)}\right)^{(n-1)} \rho\right) \\ &= \frac{1}{1-n} \log_d \left(\left(d^{(|\mathcal{G}|-N)}\right)^{(n-1)}\right) = N - |\mathcal{G}|. \end{aligned} \tag{2.21}$$

Notice that this agrees with Eq. 2.16 for the case where the subsystem A is the entire system: $|A| = N$ and $\mathcal{G}_A = \mathcal{G}$. Thus $S_n = N$ for a completely mixed state, and $S_n = 0$ for a pure state.

There are many similarities between pure and mixed states, as their density matrix is defined via $\mathcal{G}$ in much the same way. However, measurements can now reveal new information about the state, increasing its purity. In this formalism, the measurement results are not actually recorded. However it is important to note that this models a system in which the measurement results are recorded, and these will decrease the statistical uncertainty of the system. We need to determine when and how this happens.

Let the generating set $\mathcal{G}$ define a mixed state. When we perform a Z measurement, the density matrix ρ transforms as

$$\rho \mapsto \frac{P_Z \rho P_Z}{\mathrm{Tr}(P_Z \rho P_Z)} \tag{2.22}$$

There are three possibilities. The first possibility is that not all generators g commute with Z. We follow the prescription for pure states, and manipulate the generators until all but one commutes with Z. Call this noncommuting generator g^*. Then,

$$\begin{aligned} P_Z \rho P_Z = P_Z \left(d^{|\mathcal{G}|-N} P_{g^*} \prod_{g \neq g^*} P_g\right) P_Z &= d^{|\mathcal{G}|-N} \left(\prod_{g \neq g^*} P_g\right) (P_Z P_{g^*} P_Z) \\ &\propto d^{|\mathcal{G}|-N} \left(\prod_{g \neq g^*} P_g\right) P_Z = d^{|\mathcal{G}|-N} \prod_{g \in \mathcal{G}'} P_g \end{aligned} \tag{2.23}$$

where the set $\mathcal{G}'$ is the set $\mathcal{G}$ with g^* replaced with Z. This proves that when there is at least one noncommuting generator, the procedure is the same as it is for pure states: manipulate the generating set until only one generator does not commute with Z, and then replace that generator with Z.

The second possibility is that all generators commute with Z. Then,

$$P_Z \rho P_Z = \rho P_Z = d^{|\mathcal{G}|-N} \prod_{g \in \mathcal{G}'} P_g$$

where the set $\mathcal{G}'$ is the set $\mathcal{G}$ with the additional element Z. The denominator of Eq. 2.22 forces the trace of the new density matrix to equal 1, and thus the new density matrix is $d^{|\mathcal{G}'|-N} \prod_{g \in \mathcal{G}'} P_g$. In this case, the generating set gets larger, and we have learned new information about the system.

However, there is a catch. The third possibility is that all of the generators commute with Z, but Z is already an element of $\mathcal{S}$, if not of $\mathcal{G}$. In this case, we can choose a generating set that already contains Z, and the density matrix will not change after measurement. In this case, we do not learn any new information about the state.

Thus, we have the following process. If there are some generators which do not commute with Z, then perform the measurement algorithm as normal. If all generators commute with Z, then first determine if Z can be generated by the generating set. In practice, this means finding if $\vec{r}(Z)$ is in the row space of the check matrix of $\mathcal{G}$. If it is, then the state does not change. If it is not, then Z is added to the list of generators. With this we can apply our dynamics to mixed states, and calculate the total entropy.

2.7 Methodology and Results

We are now in a position to describe the implementation of the above methods and share the results.

A diagram of our procedure is shown in Fig. 2.1. We begin with an initial trivial state. For pure states, this is a product state in which every site is a Z eigenstate. For mixed states, this is a completely mixed state which contains no information about the system. The dynamics

involve the application of two-site Clifford unitary gates and projective measurements. First, the Clifford operations are applied on pairs of qudits. Next, each qudit is measured in the Z basis with a probability p which is constant throughout the procedure. Then, Clifford operations are applied again, but to the alternate pairing of sites. We use periodic boundary conditions throughout, so that site N and 1 form a pair at this step. Lastly, we again apply a Z measurement with probability p at each site. These four processes together constitute a single time step.

For pure states, the subsystem entanglement entropy $S_n(A)$ and normalized length distribution $D_{\mathcal{G}}(L)$ evolve as more time steps are applied. After the application of a sufficient number of time steps, these two functions no longer evolve with time except for small fluctuations. At this point the system has reached a steady state. The subsystem entanglement entropy and the normalized stabilizer length distribution are calculated using the methods outlined in the previous section. This process is repeated for an ensemble of systems, and we find the ensemble average of the entanglement entropy and length distribution. This is a pure state ensemble and not a statistical ensemble, as the quantum states are always known. After a large number of such systems are realized and the average taken, the value of p is changed and the process repeated.

For mixed states, our simulations do not necessarily reach a steady state. The total entropy of the system decreases monotonically with time, and thus the system will always eventually become a pure state. Rather, we detect a phase transition based on how long the mixed state takes to purify. Systems in the expected mixed phase will purify on time scales which are exponential in system size N [4]. We thus apply a number of time steps equal to the system size N, and then measure the total entropy of the final state. This process is repeated for an ensemble of systems, and we find the ensemble average of the total entropy. We still do not view this as a statistical ensemble in the usual sense, but rather view this as ensemble of states which are not necessarily exactly known and are given an equal weight to be averaged over.

The above procedures were implemented numerically in MATLAB, where each state is

represented as a $N \times 2N$ matrix for various system sizes N. This code was executed on the 'klone' cluster of the University of Washington's high performance computing resource, Hyak. The systems were evolved in parallel, over the span of weeks. For pure states, most larger system sizes ($N \geq 500$) have on the order of 1,500 realizations which are averaged over, while smaller system sizes have on the order of 15,000 to 20,000 realizations. For mixed states, each state must be evolved for more time steps, and each time step is more computationally demanding. Most larger system sizes ($N \geq 500$) have on the order of 200 to 400 realizations which are averaged over, while the $N = 250$ systems have on the order of 9,000 realizations.

2.7.1 Summary of Results

The primary results follow. We studied systems in which $d = 3$, 5, and 97. First, we find that the phase transition persists in each case that was studied. The critical value p_c of the transition increases monotonically as d increases, and seems to approach $p_c = 0.5$ for large d. This is consistent with an analytical $d \to \infty$ expansion of a circuit with Haar-random unitaries in Ref. [25]. We also perform a data collapse for the half-system subsystem entropy $S(\frac{N}{2})$, and find that for each d the correlation length exponent ν is approximately equal to 1.3.

For the purity, we find that the purification transition exists in the systems we studied. Further, it seems that the transition happens at the same critical value as the entanglement transition.

What follows are the data of our calculations, the graphs supporting our conclusions, and a discussion of their relevance.

2.7.2 Reaching the Steady-State

First we focus on pure states. Since we want to measure the entanglement entropy after the system has reached a steady state, we must determine how many time steps are required before the steady state is reached. We do this by calculating subsystem entanglement entropy after every time step to identify how long it takes before it stabilizes to a constant value. Specifically, we look at the entropy for regions which are half the total system size, $S(\frac{N}{2})$,

as a function of time. It is seen numerically that for every L, $S(L)$ converges to a constant value after the same sufficient number of time steps, and the length distribution $D_{\mathcal{G}}(L)$ also converges in the same time period. Results for $d = 2$, 3, 5, and 97 are shown in Fig. 2.2.

From these graphs we can make some helpful insights which determine how many time steps should be applied to each system; in particular, the steady state is reached for times on the order of $N/3$ and this number decreases with increasing d. In addition, for a fixed d, the number of necessary time steps is largely independent of p.

2.7.3 Pure States: Entanglement Entropy and Length Distribution

The first method for differentiating the phases is to look at the scaling of the subsystem-averaged subsystem entanglement entropy as a function of subsystem size. The entropy $S(L)$ is found by averaging the subsystem entanglement entropy for all contiguous subsystems of length L. For small p the subsystem entanglement entropy scales as a volume-law i.e., the entropy is proportional to the length of the subsystem. For larger values of p, the entropy scales as an area-law and reaches a constant value which is independent of L. At the critical point p_c which separates the two phases, the entanglement entropy scales in proportion to the logarithm of the subsystem size.

An example of this behavior is shown in Fig. 2.3. This data is from a system with $d = 3$ and system size $N = 500$. Finding the subsystem entropy always involves splitting the system into two parts. Because we have taken periodic boundary conditions, both parts are contiguous, and thus $S(L) = S(N - L)$. Therefore we only plot $S(L)$ up to length $L = N/2$.

We see all three behaviors in this plot. For low p, $S(L)$ is linear for medium sized subsystems, indicating a volume-law phase. For large p, the entropy saturates to a constant value, indicating an area-law phase. Near the critical value, $p_c \approx 0.28$, the entropy increases slowly, approximating a logarithm $S \propto \log(L)$.

Using the half-system entropy, $S(\frac{N}{2})$, we are able to perform a finite-size data collapse. One of the consequences of renormalization group theory is the prediction that for continuous phase transitions, certain thermodynamic observables Q will have a special dependence near

the phase transition. For finite system size N and temperature T, $Q(N,T)$ can generally depend on N and T in an arbitrary way. However, near the critical temperature T_c, the observable should behave as [31]

$$Q(N,T) = L^{\kappa/\nu}\, f(tN^{1/\nu}) \tag{2.24}$$

where $t = (T - T_c)/T_c$ is the reduced temperature, and κ and ν are critical exponents. The intuition comes from the fact that near the critical point the system is expected to become scale invariant. Thus, when approaching the critical point, it is expected that a change in reduced temperature can be compensated for by a change in the length scale. The combination $tN^{1/\nu}$ allows these two variables to compensate for each other in such a way.

For our model, the measurement parameter p takes on the role of temperature. We find in our systems that [1]

$$S(\tfrac{N}{2}) - S_{crit}(\tfrac{N}{2}) \;\sim\; f\left((p-p_c)N^{1/\nu}\right), \tag{2.25}$$

where $S_{crit}(\frac{N}{2})$ is the value of $S(\frac{N}{2})$ at $p = p_c$. With this scaling form, we can extract a value for the correlation length exponent ν from our data.

The results for $d = 3$, 5, and 97 are shown in Figs. 2.4, 2.5, and 2.6 respectively. In each case, we find a data collapse of the variables, and plot the best fit. There are a variety of ways to fit the data collapse, and no rigorous standard has been adopted. To find the best fit values for our data, we fitted the data to a fifth order polynomial and calculated the error for various values of p_c and ν, then chose the parameters that minimized the error. The results of this are shown in Table 2.1.

There are a few interesting consequences of these data. Many papers related to hybrid dynamics for a one-dimensional system find a connection to the universality class of percolation in two dimensions [3, 25, 26, 32, 33, 34]. However, the percolation transition is not expected to describe Clifford circuits [25] or qudits with finite d [27]. In spite of this, the two-dimensional percolation transition correlation length exponent of $\nu = 4/3$ is close to our measured $\nu \approx 1.3$ in each case. In addition, the authors in Refs. [25, 32] find that for qudit

d	p_c	ν
2	0.16	1.3
3	0.28(1)	1.30(5)
5	0.38(1)	1.29(5)
97	0.496(2)	1.29(5)

Table 2.1: Table of numerical results. The data here are based on the graphs of Figs 2.4, 2.5, and 2.6. The $d = 2$ data is taken from Ref. [1]. p_c and ν are found using a data collapse of the half-system entropy $S(\frac{N}{2})$ as a function of $(p - p_c)N^{1/\nu}$, as described in the text. The reported values for p_c and ν give the smallest error when fitting a fifth order polynomial to the collapsed data. Note that ν has a relatively smaller effect on the collapse than p_c, and thus the uncertainties are larger.

circuits with Haar random unitary gates, the critical value p_c should increase monotonically with d; this is in agreement with our calculated p_c values for the systems we studied.

The normalized stabilizer length distribution $D_{\mathcal{G}}(L)$ gives us an additional method of finding the location of the phase transition. This is because in the volume-law phase, $D_{\mathcal{G}}(L)$ has a prominent peak at $L = N/2$. Heuristically, since the clipped gauge only allows two generator endpoints per site, this is the longest that all generators can be simultaneously, leading to maximal entanglement. Starting at $p = 0$, all generators have length $N/2$ in the steady state. As p increases, this peak broadens and eventually disappears. The disappearance of this peak centered at $L = N/2$ is indicative of the phase transition.

The graphs for $d = 3$, 5, and 97 are shown in Figs. 2.7, 2.8, and 2.9 respectively. These graphs also show the characteristic falloff of the stabilizer lengths as being proportional to $1/L^2$ in the volume-law phase i.e., at small p values. In the area-law phase, this is modified by an exponential falloff which is dependent on p.

2.7.4 Mixed States: Purity and Total Entropy

The last quantity we calculate in this model is the purity of the system. The total entropy of an individual system monotonically decreases; we cannot lose information about the system once we have gained it. Thus, we do not find a steady state in these systems. Rather, we evolve a completely mixed state of N qudits by N time steps, and then measure the total entropy of the resulting density matrix.

The results for d = 3, 5, and 97 are shown in Figs. 2.10, 2.11, and 2.12, respectively. Our main result is that the phase transition persists for all values of d that we studied, and that the critical value p_c of this transition is at the same critical value as the system's entanglement transition.

The difference between the purifying phase and the mixed phase of a system is in how long the system takes to purify. For small values of p, the system is in the mixed phase. The number of time steps it takes for the total entropy S_n to become zero is much longer than the system size N. Thus, the total entropy is not zero after N time steps. For large values of p, the system is in the purifying phase. The measurements are able to purify the system in a number of steps less than the system size N, and thus the total entropy is zero after N time steps.

From a quantum information perspective, the total entropy S_n represents the amount of quantum information that the state is able to hide from the measurements. In the mixed phase, the measurements occur infrequently enough that the system can protect some quantum information from the outside measurements. Because of the unitary operations, this quantum information becomes spread over enough of the system that the local measurements cannot access it [4]. In the purifying phase, the measurements happen frequently enough that the system cannot protect any quantum information.

2.8 Discussion

We have generalized a well-known class of entanglement transitions to qudits of prime order d. We have shown that the characteristic phase transition of this model is robust to changes in on-site Hilbert space dimension. In addition, we give evidence that the critical value p_c of the transition increases with increasing d, and approaches $p_c = 0.5$ in the large-d limit. We extracted the correlation length exponents of these transitions, and found that they are all consistent with $\nu \approx 1.3$, which is close to the correlation length exponent of the bond percolation transition of $\nu = 4/3$. This is surprising, as the universality class of Clifford circuits on qudits is not expected to be described by the percolation universality class [27, 25]. A complete description, or even identification, of the Clifford CFT remains to be seen. It is therefore beneficial to know that the critical exponent ν seems to stay constant at finite values of d.

We also studied the purity dynamics of these systems by calculating the total entropy after N time steps. We found that the purification transition also exists, and for the systems studied it occurs at the same critical rate of measurement as the entanglement transition. It is not clear *a priori* that the two transitions would need to be related in this way, and this represents more evidence that the two are in fact linked in the case of Clifford unitary evolution.

This work was facilitated through the use of advanced computational, storage, and networking infrastructure provided by the Hyak supercomputer system and funded by the Student Technology Fee at the University of Washington.

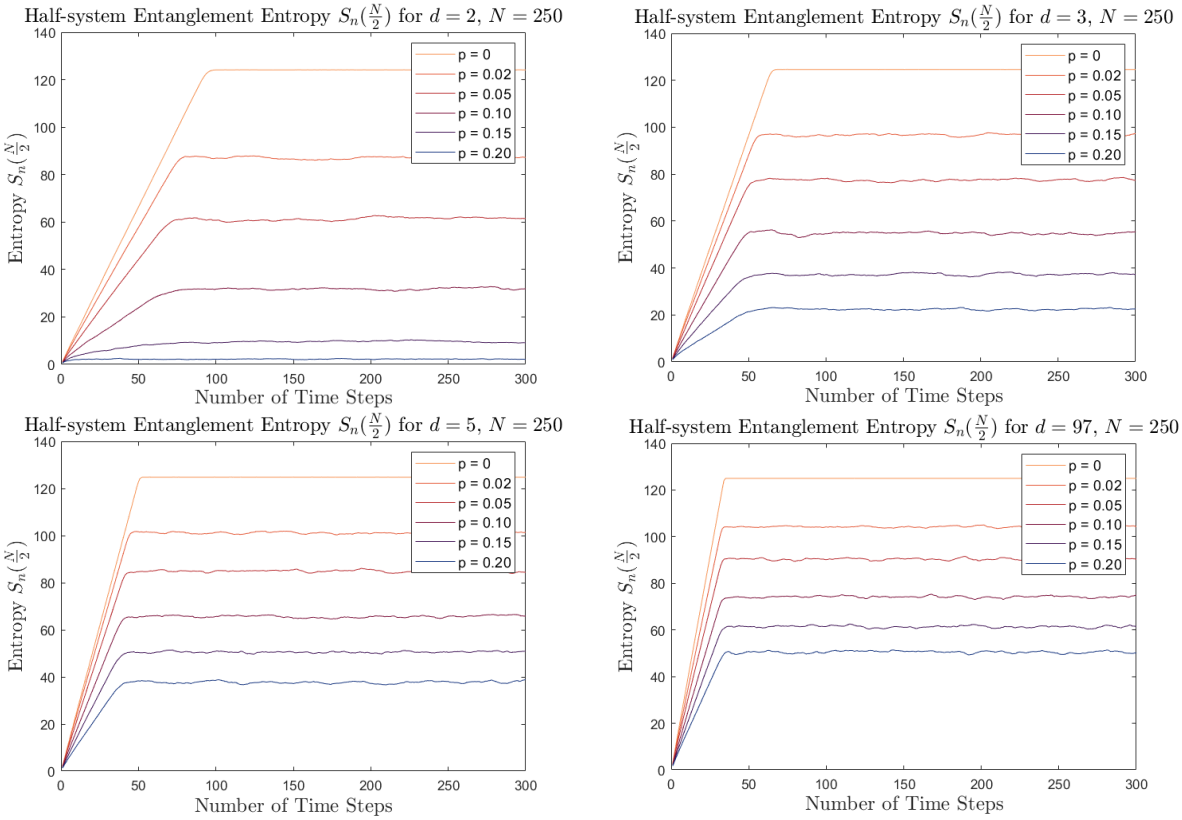

Figure 2.2: Graph of subsystem entropy versus time for subsystems of size $N/2$ in systems of size $N = 250$ with various values of d. Different colors represent different values of measurement probability p. All points represent the average of 20 realizations. Entanglement between two halves of the system reaches a constant value after a sufficient number of time steps, which is indicative of a steady state as described in the text. We see that the half-system entanglement entropy increases linearly with time until reaching a steady value after a time $T << N$, which is a general rule for other system sizes. The stabilizer length distribution also attains a steady profile after the same time period. Note that the system reaches a steady state more quickly with larger values of d, and that for a fixed p, the entropy of the steady state increases with larger values of d.

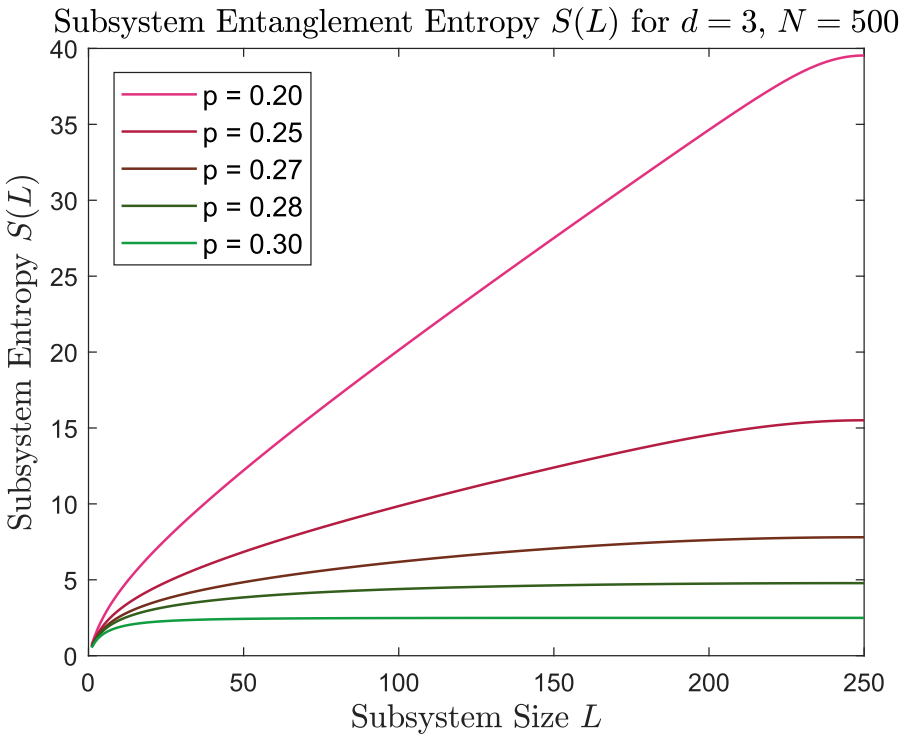

Figure 2.3: The bipartite subsystem entanglement entropy $S(L)$ between the average contiguous region of size L and the rest of the system for qubits of order $d = 3$. The Rényi entropies S_n used here are defined in Eq. 2.12 and are identical for all $n \geq 1$. Note that separating a contiguous subsystem splits the system into two parts, which implies $S(L) = S(N - L)$; thus we only plot values for L up to $N/2$. Different colors represent different values of the measurement probability p. The phase transition occurs around $p \approx 0.28$. In the low-p phase, the subsystem entanglement entropy increases linearly; the entropy is proportional to the "volume" L of the one-dimensional subsystem, and thus the entropy scales as a volume-law. In the high-p phase, the subsystem entanglement entropy reaches a constant value that is independent of the subsystem size L. This is thus proportional to the "area" of the subsystem, and thus the entropy scales as an area-law. Near the critical point $p_c \approx 0.28$, the subsystem entanglement entropy increases logarithmically with subsystem size L, which is indicative of a critical phase that separates the volume-law and area-law phases.

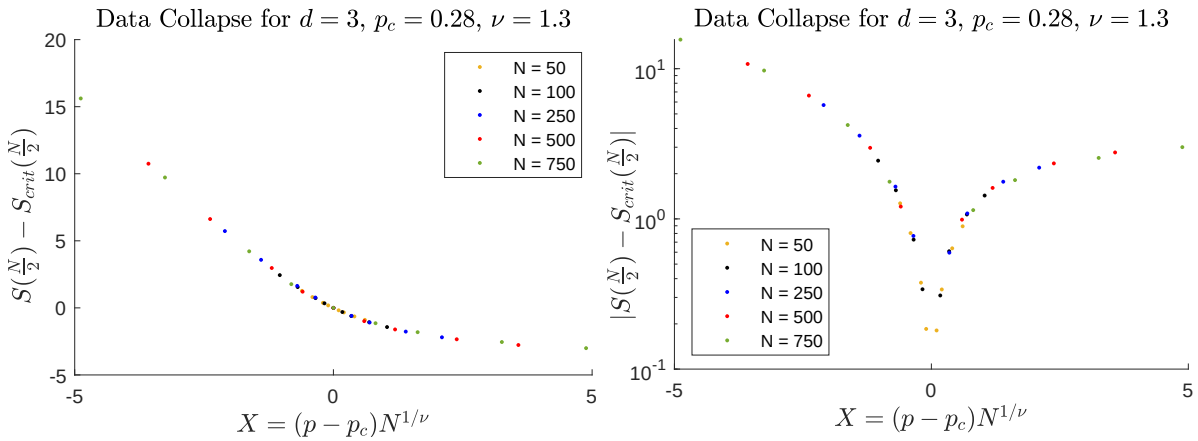

Figure 2.4: Data collapse for $d = 3$. The vertical axis gives the average Rényi entropy between two equal halves of the subsystem, $S(\frac{N}{2})$, normalized to be zero at the critical value $p_c = 0.28$ by subtracting the entropy at the critical value, $S_{crit}(\frac{N}{2})$. The Rényi entropies S_n defined in Eq. 2.12 are identical for all $n \geq 1$. Renormalization group considerations imply that there should exist thermodynamic quantities which are a function of a special combination of variables as in Eq. (2.24). From this, we can extract the critical value $p_c \approx 0.28$ and the correlation length exponent $\nu \approx 1.3$. These values were extracted by fitting the above data to a fifth order polynomial, and finding the values of p_c, ν which minimized the error of the fit. The figure on the right is the absolute value of the same data, plotted with a logarithmic scale on the vertical axis. This highlights how well the data collapses near the critical point.

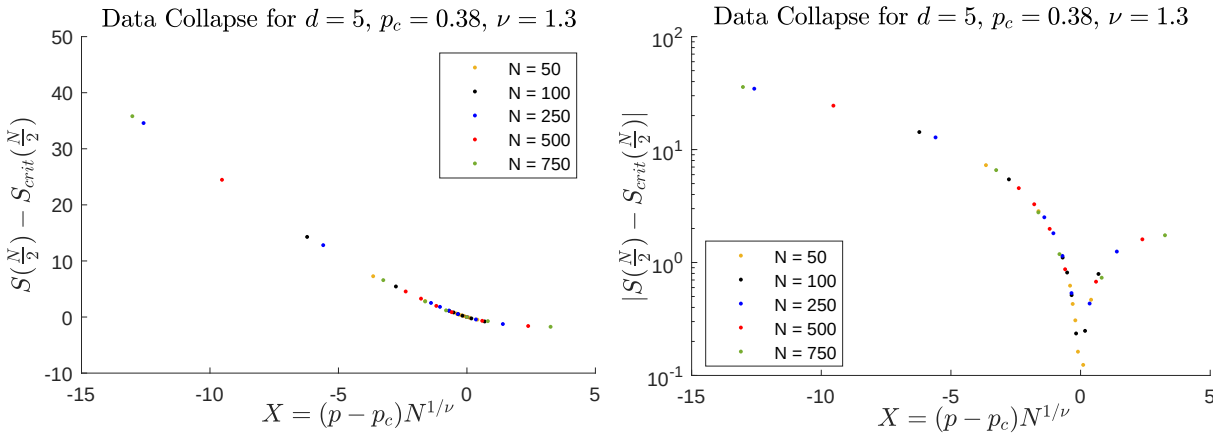

Figure 2.5: Data collapse for $d = 5$. The vertical axis gives the average Rényi entropy between two equal halves of the subsystem, $S(\frac{N}{2})$, normalized to be zero at the critical value $p_c = 0.38$ by subtracting the entropy at the critical value, $S_{crit}(\frac{N}{2})$. The Rényi entropies S_n defined in Eq. 2.12 are identical for all $n \geq 1$. Renormalization group considerations imply that there should exist thermodynamic quantities which are a function of a special combination of variables as in Eq. (2.24). From this, we can extract the critical value $p_c \approx 0.38$ and the correlation length exponent $\nu \approx 1.3$. These values were extracted by fitting the above data to a fifth order polynomial, and finding the values of p_c, ν which minimized the error of the fit. The figure on the right is the absolute value of the same data, plotted with a logarithmic scale on the vertical axis. This highlights how well the data collapses near the critical point.

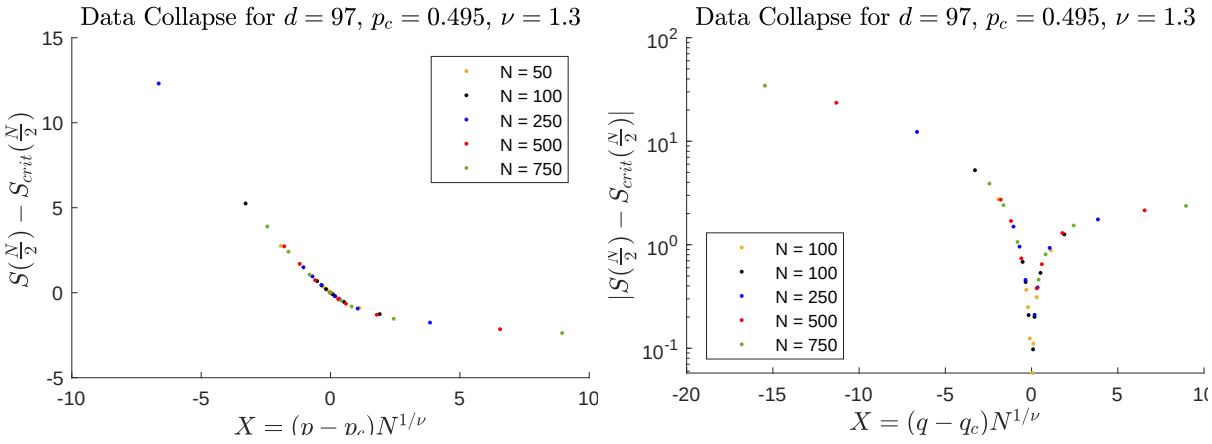

Figure 2.6: Data collapse for $d = 97$. The vertical axis gives the average Rényi entropy between two equal halves of the subsystem, $S(\frac{N}{2})$, normalized to be zero at the critical value $p_c = 0.495$ by subtracting the entropy at the critical value, $S_{crit}(\frac{N}{2})$. The Rényi entropies S_n defined in Eq. 2.12 are identical for all $n \geq 1$. Renormalization group considerations imply that there should exist thermodynamic quantities which are a function of a special combination of variables as in Eq. (2.24). From this, we can extract the critical value $p_c \approx 0.495$ and the correlation length exponent $\nu \approx 1.3$. These values were extracted by fitting the above data to a fifth order polynomial, and finding the values of p_c, ν which minimized the error of the fit. The figure on the right is the absolute value of the same data, plotted with a logarithmic scale on the vertical axis. This highlights how well the data collapses near the critical point.

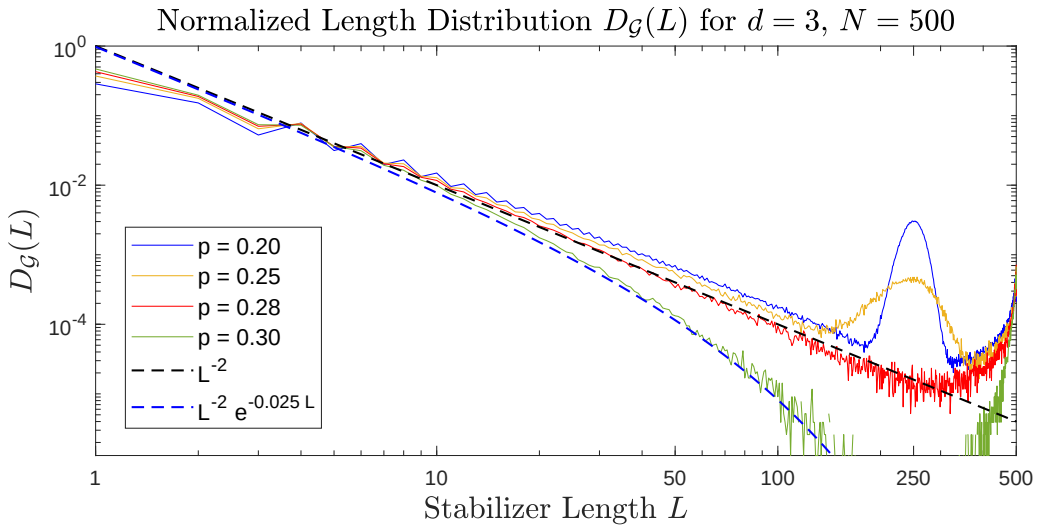

Figure 2.7: Graph of the normalized stabilizer length distribution $D_{\mathcal{G}}(L)$ versus stabilizer length L for system size $N = 500$ with $d = 3$. The value of $D_{\mathcal{G}}(L)$ is $1/N$ times the average number of stabilizers that are supported on regions of size L. Different colors represent different values of measurement probability p. The critical value of p occurs around $p_c \approx 0.28$, and is indicated by the disappearance of the bump in the graph centered at $N/2$. We can see in the low-p volume-law phase that the normalized length distribution function follows the profile $D_{\mathcal{G}}(L) \propto L^{-2}$ for small values of L. In the high-p area-law phase, this is modified by an exponential damping factor, with a p-dependent falloff coefficient.

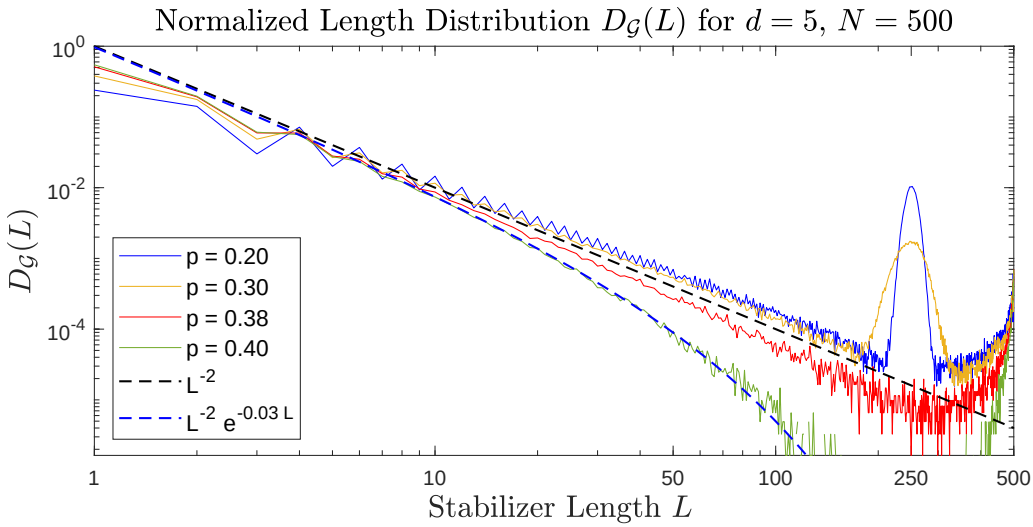

Figure 2.8: Graph of the normalized stabilizer length distribution $D_{\mathcal{G}}(L)$ versus stabilizer length L for system size $N = 500$ and $d = 5$. The value of $D_{\mathcal{G}}(L)$ is $1/N$ times the average number of stabilizers that are supported on regions of size L. Different colors represent different values of measurement probability p. The critical value of p occurs around $p_c \approx 0.38$, and is indicated by the disappearance of the bump in the graph centered at $N/2$. We can see in the low-p volume-law phase that the normalized length distribution function follows the profile $D_{\mathcal{G}}(L) \propto L^{-2}$ for small values of L. In the high-p area-law phase, this is modified by an exponential damping factor, with a p-dependent falloff coefficient.

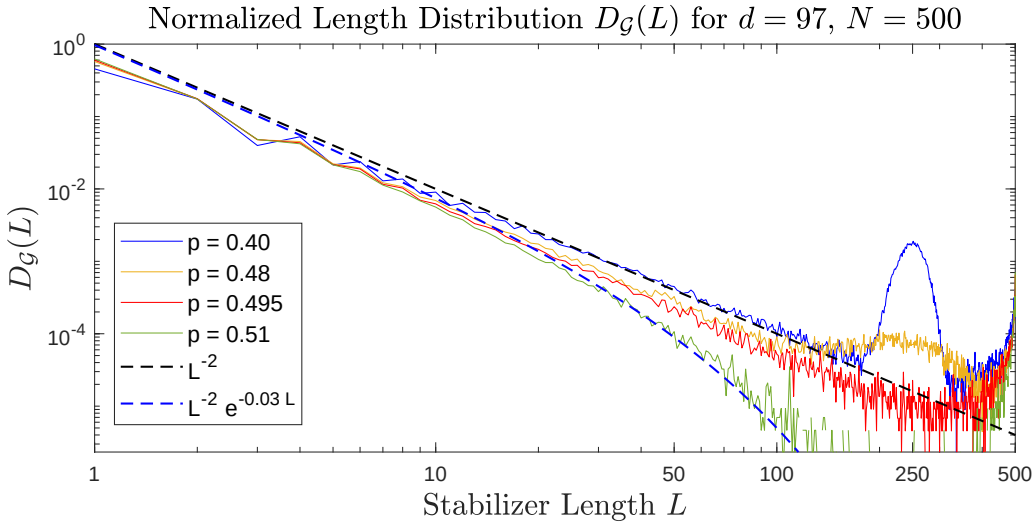

Figure 2.9: Graph of the normalized stabilizer length distribution $D_{\mathcal{G}}(L)$ versus stabilizer length L for system size $N = 500$ and $d = 97$. The value of $D_{\mathcal{G}}(L)$ is $1/N$ times the average number of stabilizers that are supported on regions of size L. Different colors represent different values of measurement probability p. The critical value of p occurs around $p_c \approx 0.495$. We can see in the low-p volume-law phase that the normalized length distribution function follows the profile $D_{\mathcal{G}}(L) \propto L^{-2}$ for small values of L. In the high-p area-law phase, this is modified by an exponential damping factor, with a p-dependent falloff coefficient.

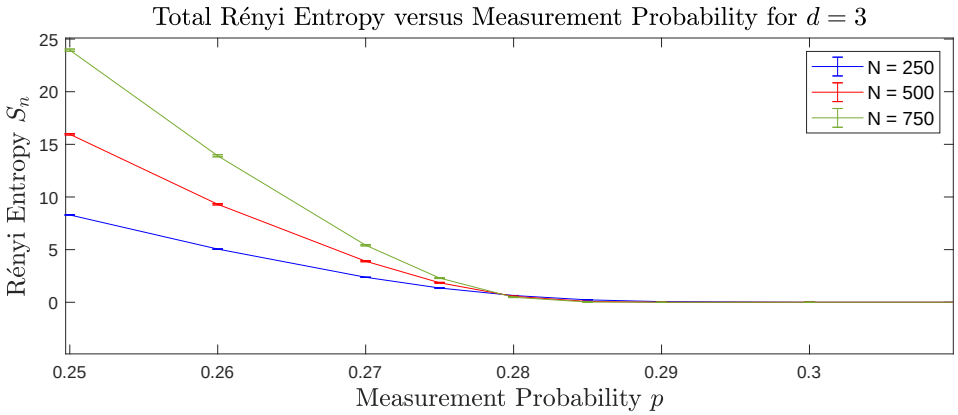

Figure 2.10: The statistical Rényi entropy S_n after N time steps versus measurement probability p for mixed systems with $d = 3$. The Rényi entropies S_n defined in Eq. 2.12 are identical for all $n \geq 1$. Because the system is generally not a pure state, no subsystems are taken and the full density matrix is used to calculate S_n. For small values of p, the measurements do not happen frequently enough to purify the state, and the state is still mixed after N time steps. This is indicative of a "mixed" phase in which measurements require a number of time steps exponential in N to purify the state. For large values of p, the measurements are able to purify the state within N time steps and the final Rényi entropy is zero. The purification transition occurs at $p_c \approx 0.28$, the same value as the entanglement transition for $d = 3$.

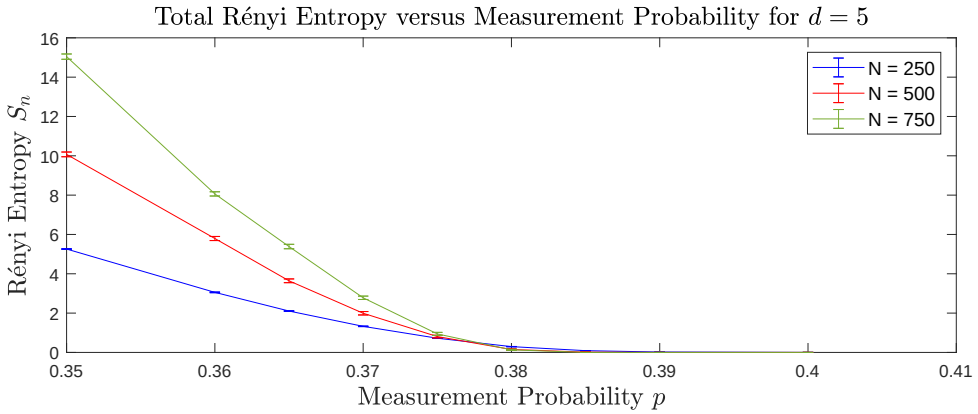

Figure 2.11: The statistical Rényi entropy S_n after N time steps versus measurement probability p for mixed systems with $d = 5$. The Rényi entropies S_n defined in Eq. 2.12 are identical for all $n \geq 1$. Because the system is generally not a pure state, no subsystems are taken and the full density matrix is used to calculate S_n. For small values of p, the measurements do not happen frequently enough to purify the state, and the state is still mixed after N time steps. This is indicative of a "mixed" phase in which measurements require a number of time steps exponential in N to purify the state. For large values of p, the measurements are able to purify the state within N time steps and the final Rényi entropy is zero. The purification transition occurs at $p_c \approx 0.38$, the same value as the entanglement transition for $d = 5$.

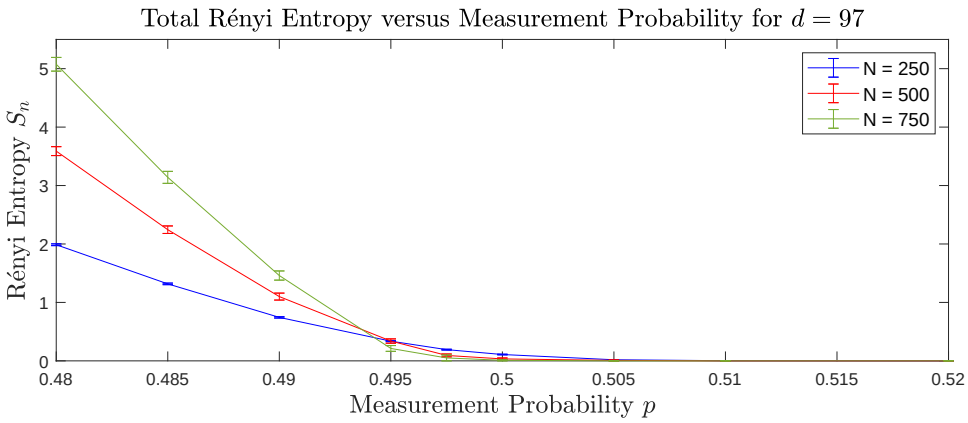

Figure 2.12: The statistical Rényi entropy S_n after N time steps versus measurement probability p for mixed systems with $d = 97$. The Rényi entropies S_n defined in Eq. 2.12 are identical for all $n \geq 1$. Because the system is generally not a pure state, no subsystems are taken and the full density matrix is used to calculate S_n. For small values of p, the measurements do not happen frequently enough to purify the state, and the state is still mixed after N time steps. This is indicative of a "mixed" phase in which measurements require a number of time steps exponential in N to purify the state. For large values of p, the measurements are able to purify the state within N time steps and the final Rényi entropy is zero. The purification transition occurs at $p_c \approx 0.495$, the same value as the entanglement transition for $d = 97$.

Chapter 3

FREE FERMION PURIFICATION TRANSITIONS

In this chapter, we focus on the purification properties of free fermion systems. We do this by expanding the scope of a known purification transition involving a one-dimensional system of Majorana fermions. While the entanglement properties of monitored free fermions have been studied extensively, purification is not as well understood [5], and there are still many open questions in this field.

To advance this knowledge, we apply hybrid dynamics to a one-dimensional system of Majorana fermions; these dynamics involve unitary gates acting on pairs of Majorana fermions, and measurements projecting onto pairs of Majorana fermions. Both of these operations have an associated probability, which can be varied to probe a phase diagram for the system. Under a particular choice of unitary gates, namely gates which interchange pairs of Majorana fermions, this system reduces exactly to a classical statistical mechanics model known as the completely packed loop model with crossings (CPLC). In this model, a phase transition is known to exist, although it has a different interpretation. The free fermion unitary gates are viewed as a generalization of this model, and this allows us to probe the robustness of the model and its associated phase transitions.

We unveil a phase transition between a "mixed" phase, which has area-law behavior, and a critical "Goldstone" phase in which the entropy increases logarithmically with system size [16]. Furthermore, we demonstrate the robustness of the transition by finding a phase diagram of the model, which retains some of the properties of a corresponding phase diagram of the CPLC. However, there are additional nontrivial features which are introduced. In particular, there exists an enhanced symmetry in the CPLC which exists on the edges of the phase diagram, and prevents a phase transition at those extremes. This restriction is lifted in

our model, and we find a phase transition where the original model had none. We extract the critical exponents at various points along the phase transition line, but can neither confirm nor rule out the possibility that our model shares the universality class of the original CPLC phase transitions.

3.1 Introduction

Recently the study of hybrid quantum circuits, involving both unitary dynamics and projective measurements, has received a great deal of attention [1, 3, 27]. By focusing on the ensemble of quantum trajectories of pure states defined by the various measurement outcomes, one can study new types of nonequilibrium phase transitions, with the canonical example being the entanglement transition. In the entanglement transition, the ensemble-averaged subsystem entanglement entropy changes behavior as the measurement rate is increased. For low measurement rates, the system exhibits a *volume-law* phase where the subsystem entanglement entropy increases in proportion to the size of the subsystem, while for higher measurement rates the system exhibits an *area-law* phase where the subsystem entanglement entropy increases in proportion to the size of the boundary of the subsystem.

A closely related concept is that of a "purification" transition, where instead of pure quantum state trajectories one studies the purifying behavior of an initial maximally mixed state as the rate of measurement is varied. For low measurement rates, the system generally exhibits a *mixed* phase where the system stays mixed for times which are parametrically long in system size [4], while for high measurement rates the system exhibits a *purifying* phase in which the measurements evolve the system into a pure state on a relatively short timescale. Note that this mixed phase and purifying phase correspond to the volume-law and area-law phases, respectively, for the entanglement transition. In fact, for many systems in the mixed phase, the system exhibits a type of volume-law behavior where the final entropy increases in proportion to the size of the system.

In the special case of free fermion dynamics [26], in which measurements are only of Fock space fermion mode occupation numbers and unitary operations are exponentials of bilinears

of the creation and annihilation operators, the volume-law-like mixed phase is known to be unstable to any non-zero measurement rate [8, 35]. However, such free fermion dynamics can still accommodate an interesting phase transition from a purifying phase to a so-called "Goldstone" phase [2]. The latter still exhibits purifying behavior, but on time scales parametrically longer in system size. More precisely, in the Goldstone phase the entropy for a system of length L after a time of order L scales as $\log L$, whereas in the purifying phase this entropy would be close to 0 i.e., the state would have approximately purified long before this time scale was reached. This phase transition can be realized in a specific free fermion model, one that can be solved [36] by exact mapping to a known statistical mechanical model, the completely packed loop model with crossings (CPLC) [2].

A natural question one may ask is, how generic is the CPLC phase diagram in the context of free fermion hybrid dynamics? In other words, do the purifying and Goldstone phases persist when the dynamics of this specific free fermion model are deformed slightly away from the point that is dual to the CPLC? Is the phase transition still continuous, and is it in the same universality class as that of the CPLC?

In this chapter, we investigate these questions by extending the CPLC-dual free fermion model to a more general family of free fermion models. We follow Ref. [36] and observe that the CPLC-dual model has a convenient description in terms of a one-dimensional chain of Majorana fermions. This mapping has unitary gates that swap neighboring pairs of Majorana fermions and measurements which project onto the occupation number of a free fermion mode defined by a neighboring pair of Majorana operators. These gates are implemented with respect to one pairing of Majorana operators and its complementary pairing in an alternating fashion, as described in detail below. The phase diagram is a function of two parameters, p and q, which control the rate of measurements and the asymmetry between measurements of the two complementary pairings of Majorana modes, respectively. Our generalized model replaces the unitary SWAP gate, which may be thought of as a $\frac{\pi}{2}$ rotation in the SO(2) group rotating γ_1 into γ_2, by a rotation by a random angle inside this SO(2). The measurement gates are as in the CPLC, and the phase diagram is once again a function

of the two parameters p and q.

Our generalized model no longer admits an easily solvable statistical mechanical dual, although in principle some statistical mechanical dual should exist, as discussed below. Therefore to study it, we instead leverage the free fermion nature of the dynamics to perform efficient Monte Carlo simulations using the Gaussian state formalism. The essential feature of both the CPLC and our generalized models which makes this possible is the fact that, for a particular quantum trajectory, the many-body quantum state of $2N$ Majorana fermions remains Gaussian, meaning that it can be efficiently encoded in a correlation matrix with $O(N^2)$ entries. This allows us to avoid having to simulate dynamics in a Hilbert space exponentially large in N.

We find that the general features of the CPLC phase diagram persist in the generalized model. The area-law and Goldstone phases remain, but the phase transition between them shifts. An important qualitative difference is that the Goldstone phase persists down to finite $p < 1$ for $q = 0,\ 1$ in the generalized model, in contrast to the CPLC. This implies that the unitaries in the generalized model are more scrambling in some sense than those of the CPLC, because they can support the Goldstone phase with commuting measurements (i.e., at $q = 0,\ 1$). The CPLC, on the other hand, requires non-commuting measurements [11, 37, 38, 39] to support the Goldstone phase. Our result is consistent with the result that a volume-law entanglement cannot be maintained in free fermion systems at finite measurement rates [35, 8], comports with the results found in Ref. [40] in the case of continuous monitoring, and bears resemblance to the results of Refs. [12, 41] in the case of non-unitary free fermion evolution; see also Ref. [9] for additional exploration of free fermion phases and phase transitions with weak measurements, and Refs. [42, 43] for further study of the phase transition from an area-law phase to a logarithmic phase. We would also like to note that the transitions found in the CPLC have also been studied using entanglement negativity and other measures in the context of monitored dynamics in Ref. [33].

We also perform a finite size scaling analysis that allows us to extract a correlation length critical exponent $\nu \approx 2.4$ for the generic transition between the two phases. The accuracy

of our analysis is not sufficient to definitively conclude that this corresponds to a different universality class from the CPLC, which has $\nu_{\mathrm{CPLC}} \approx 2.75$ [2].

The rest of this chapter is structured as follows. In Sec. 3.2 we review the CPLC and construct the duality mapping between this model and a model of free fermion hybrid dynamics. In particular, we highlight the connection between the "spanning number" in the CPLC and the entropy in the quantum model. In Sec. 3.3 we discuss more general free fermion models, and introduce the Gaussian state formalism that allows us to efficiently simulate them. In Sec. 3.4 we present the results of our Monte Carlo numerical simulations of the more general free fermion models. In Sec. 3.5 we summarize our results and consider future directions. In particular, we discuss a qualitative change in the shape of the phase boundary between the CPLC-dual and generalized models, and propose a symmetry-based explanation of this difference.

3.2 Mapping to the CPLC

This section outlines a particular implementation of the duality between the CPLC and a quantum model of Majorana worldlines, first proposed in Ref. [36]. We consider a one-dimensional chain of N spinless fermions, and write the operator algebra in terms of $2N$ Majorana fermions γ_k, $k = 1, \ldots, 2N$. These are related to the usual creation and annihilation operators $a_j, a_j^\dagger$, $j = 1, \ldots, N$, by:

$$\gamma_{2j-1} = a_j + a_j^\dagger \qquad a_j = \frac{1}{2}\left(\gamma_{2j-1} - i\gamma_{2j}\right)$$
$$\gamma_{2j} = i(a_j - a_j^\dagger) \qquad a_j^\dagger = \frac{1}{2}\left(\gamma_{2j-1} + i\gamma_{2j}\right)$$

These Majorana operators are unitary, hermitian, and square to the identity. Any two Majorana operators with different indices will anticommute. We have $i\gamma_{2j-1}\gamma_{2j} = (-1)^{n_j} = 1 - 2n_j$, where $n_j = a_j^\dagger a_j$ is the occupation number operator at site j, taking eigenvalues 0 and 1.

3.2.1 Hybrid unitary-measurement circuit

We take periodic boundary conditions, so that a subscript of $N+1$ below is to be interpreted as 1. The time step is labeled by a positive integer, and the protocol depends on the parity of this time step. The quantities p and q are two real numbers between 0 and 1 which serve as control parameters. For convenience, let us first define the two-Majorana unitary gate $U_{r,r+1}$, $(r = 1, \ldots, 2N)$ by

$$U_{r,r+1} = \frac{1}{\sqrt{2}} \left(1 - \gamma_r \gamma_{r+1}\right). \tag{3.1}$$

This gate acts as follows:

$$U_{r,r+1}(\gamma_r) U_{r,r+1}^{\dagger} = \gamma_{r+1}$$
$$U_{r,r+1}(\gamma_{r+1}) U_{r,r+1}^{\dagger} = -\gamma_r$$

while commuting with all γ_j such that $j \neq r, r+1$.

Odd time steps: We perform two-Majorana gates on all pairs $(2j-1, 2j)$ of nearest neighbor Majorana operators. For each such pair $(2j-1, 2j)$, the gate is chosen from three possibilities: (1) with probability p we act with $U_{2j-1,2j}$; (2) with probability $(1-p)q$ we measure $i\gamma_{2j-1}\gamma_{2j}$; (3) with probability $(1-p)(1-q)$ we do nothing i.e., act with the identity gate.

Even time steps: We perform two-Majorana gates on all complementary pairs $(2j, 2j+1)$ of nearest neighbor Majorana operators. For each such pair $(2j, 2j+1)$, the gate is chosen from three possibilities: (1) with probability p we act with $U_{2j,2j+1}$; (2) with probability $(1-p)(1-q)$ we measure $i\gamma_{2j}\gamma_{2j+1}$; (3) with probability $(1-p)q$ we do nothing i.e., act with the identity gate. Note that we have effectively exchanged $q \leftrightarrow (1-q)$ for this step.

This protocol is illustrated in Figure 3.1. The variable p determines the rate of unitary application: $p = 0$ describes a system where no $U_{r,r+1}$ gates are applied, and $p = 1$ corresponds to acting with only $U_{r,r+1}$ gates. The variable q acts as a measurement ratio describing the relative frequency of the two types of noncommuting measurements, either of the on-site pair $(2j-1, 2j)$, or the between-site pair $(2j, 2j+1)$. We note here a symmetry: with periodic

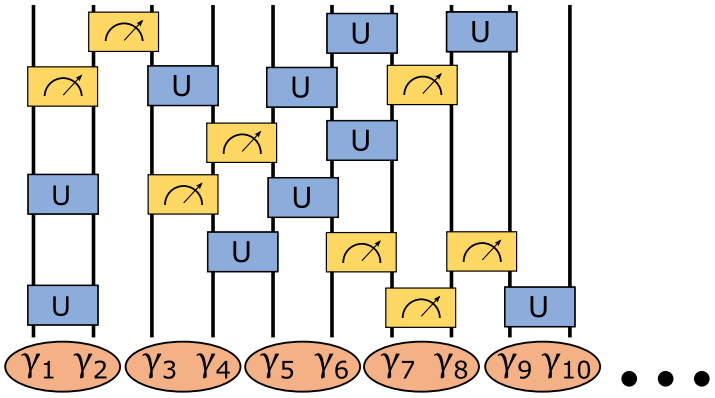

Figure 3.1: The protocol for the hybrid dynamics described in the text. The vertical direction represents time; odd and even time steps correspond to the two complementary ways of pairing neighboring Majorana operators. For each such pairing, nearest neighbor gates are applied which either perform a measurement (and record the outcome), apply a certain unitary gate, or do nothing. For odd time steps, the unitary gate is applied to a pair with probability p, and a measurement performed with probability $(1-p)q$. For even time steps, the unitary gate is applied to a pair with probability p, and a measurement performed with probability $(1-p)(1-q)$.

boundary conditions, mapping $q \to (1-q)$ is equivalent to shifting each Majorana operator by one, $\gamma_k \to \gamma_{k+1}$. Since none of the operators in the dynamics depend explicitly on the index k, this is a symmetry. Thus, the phase diagrams will have $q \leftrightarrow (1-q)$ symmetry. We expect that with open boundary conditions, the symmetry will still hold in the thermodynamic limit.

3.2.2 Connection to Completely Packed Loop Model with Crossings

Having defined our quantum model, we now describe an exact mapping to a known statistical mechanics model, the completely packed loop model with crossings (CPLC). To do this, it will be useful to introduce the notion of a fermionic stabilizer for a state in our 2^N dimensional

many-body Fock space. We define the stabilizer group of the fermionic stabilizer state $|\Psi\rangle$ in an way analogous to bosons, as defined in Sec. 2.1. We define a generating set $\mathcal{G}$ to be a set of N independent commuting Majorana bilinear operators $g = \pm i\gamma_k\gamma_l$, such that for each bilinear, $g|\Psi\rangle = +|\Psi\rangle$. Their independence implies that each Majorana operator γ_k appears exactly once in this set of bilinears. We think of two Majorana fermions with indices j and k as being paired together if the bilinear $\pm i\gamma_j\gamma_k$ is an element of the generating set. The stabilizer group is the group which is generated by multiplication of elements in this generating set, along with the identity. A state $|\Psi\rangle$ is a stabilizer state if such a set of stabilizers exist. Furthermore, a stabilizer group generated by N independent commuting Majorana bilinears will uniquely define a fermionic stabilizer state $|\Psi\rangle$, up to an overall phase. The proof for this mirrors that for the bosonic qubit case given in Sec. 2.1: the generators g are independent commuting Majorana bilinears which square to the identity, and thus the size of the stabilizer group is $2^{|\mathcal{G}|}$, and the dimensionality of the stabilized subspace is $2^{N-|\mathcal{G}|}$.

The notion of a fermionic stabilizer state is useful because it is preserved by the dynamics of this section: the quantum trajectory of an initial stabilizer state consists only of stabilizer states. To see this, let us assume that we have a stabilizer state $|\Psi\rangle$, and let us act with one time step of our dynamics, analyzing the action of each of the gates in turn. If the gate is the identity, certainly the stabilizer nature of the state is unchanged, since the state itself is unchanged. If the gate is $U_{r,r+1}$, then the effect on the algebra is to swap γ_r and γ_{r+1}, up to a sign. In particular, for any stabilizer g,

$$g|\Psi\rangle = +|\Psi\rangle \implies U_{r,r+1}|\Psi\rangle = U_{r,r+1}\left(g|\Psi\rangle\right) = \left(U_{r,r+1}gU_{r,r+1}^\dagger\right)U_{r,r+1}|\Psi\rangle = +U_{r,r+1}|\Psi\rangle$$

meaning that the new state $U_{r,r+1}|\Psi\rangle$ is stabilized by the operators $U_{r,r+1}gU_{r,r+1}^\dagger$, effectively given by exchanging γ_r and γ_{r+1}; thus the state is still a stabilizer state.

Finally, let us analyze what happens when we measure $i\gamma_r\gamma_{r+1}$. First, in the case when the Majorana fermions with indices r and $r+1$ are already paired by the stabilizers, then the state is an eigenstate of $i\gamma_r\gamma_{r+1}$. A measurement will return the eigenvalue for this bilinear but does not change the state. Now suppose that r and $r+1$ are not paired, but rather r is

paired with s and $r+1$ is paired with t; then the generating set $\mathcal{G}$ consists of $N-2$ bilinears along with the two elements $\pm i\gamma_r\gamma_s$ and $\pm i\gamma_{r+1}\gamma_t$. This means that the operator $\pm\gamma_r\gamma_s\gamma_{r+1}\gamma_t$ is in the stabilizer group generated by $\mathcal{G}$, and $|\Psi\rangle$ is an eigenstate of this operator as well. Since $i\gamma_r\gamma_{r+1}$ commutes with this operator, measuring $i\gamma_r\gamma_{r+1}$ will not change eigenvalue of $|\Psi\rangle$ under $\pm\gamma_r\gamma_s\gamma_{r+1}\gamma_t$. Thus, measurement brings $|\Psi\rangle$ to an eigenstate of both of these operators, and hence also of $i\gamma_s\gamma_t = (i\gamma_r\gamma_{r+1})(\gamma_r\gamma_s\gamma_{r+1}\gamma_t)$. The other elements of $\mathcal{G}$ also commute with $i\gamma_r\gamma_{r+1}$, and thus the new state after measurement, $|\Psi'\rangle$, is stabilized by the original $N-2$ elements of $\mathcal{G}$ along with $\pm i\gamma_r\gamma_{r+1}$ and $\pm i\gamma_s\gamma_t$. The signs of the bilinears depend on the measurement outcome, but the Majorana operator content does not. These N commuting bilinears are enough to uniquely define the state $|\Psi'\rangle$ (up to overall sign), and thus $|\Psi'\rangle$ is a fermionic stabilizer state with a stabilizer group generated by this set of bilinears. This can be seen as a type of entanglement swapping [44] between the Manorana fermions due to the joint measurement $i\gamma_r\gamma_{r+1}$.

The pairing rules so described can be tracked by representing the entanglement pairing through a configuration of loops, as in Figure 3.2. The loops can be viewed as inhabiting a checkerboard pattern of squares, corresponding to an alternating sequence of even and odd steps in time (which increases in the vertical direction). Each square of the checkerboard corresponds to a pairing of Majorana operators and has one of three different types of configurations in it: an exchange of lines (corresponding to a unitary gate), a configuration preserving the position of the lines (corresponding to doing nothing i.e., applying the identity gate), and a "capped off" configuration (corresponding to a measurement on the Majorana bilinear). Thus, by the discussion in the previous paragraph, the stabilizers of the final state are given by the pairing of the top endpoints in the diagram, as illustrated in Fig. 3.3.

The probability of each configuration occurring is the product of the various probabilities p, $(1-p)q$, and $(1-p)(1-q)$ over all the squares of the checkerboard pattern. This is just the Boltzmann weight of the completely packed loop model with crossings (CPLC) [2].

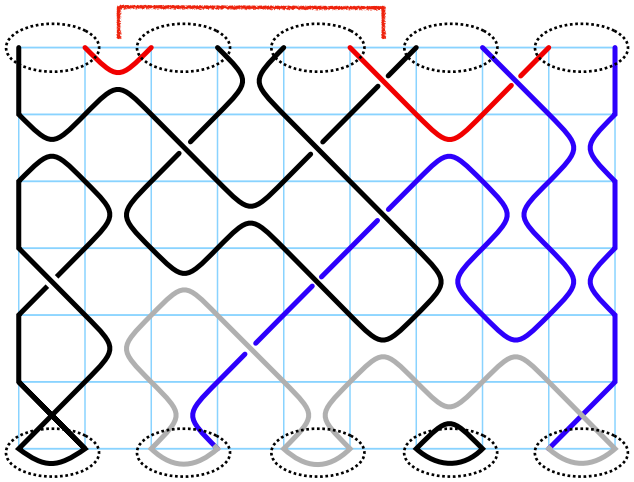

Figure 3.2: A trajectory of the circuit model with measurements, shown here with open boundary conditions. This diagram corresponds to the circuit shown in Fig. 3.1. The state is assumed to initially be an eigenstate of fermion occupation number at each site, though this need not be the case. Rotated by 45° this becomes a configuration of the completely packed loop model with crossings (CPLC). The solid thick lines represent Majorana worldlines. The spanning number n_s is given by the number of lines connecting the bottom (initial state) and top (final state) of the configuration. Here, $n_s = 2$, given by the two blue lines.

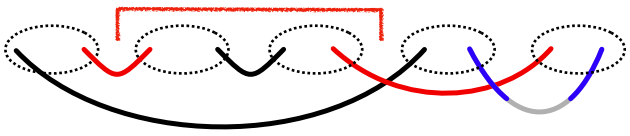

Figure 3.3: This simplified graphical view of the fermionic stabilizer state at the final time shows how the worldlines connect parts of the state in Fig. 3.2. The dotted ovals denote which Majorana operators are paired up into physical fermions. The entanglement entropy between two regions is $\frac{1}{2}\log 2$ times the number of Majorana worldlines connecting them, due to reasons similar to those for Eq. 2.17. Here, the entanglement between the second and third physical fermion (red bracket) and the rest of the system is $2 \cdot \frac{1}{2}\log 2 = \log 2$.

3.2.3 Spanning Number and Entropy

In the previous section we outlined a correspondence between a model of free fermion hybrid dynamics and the CPLC. In order for this correspondence to be useful, we have to identify corresponding observables in the two models. In the CPLC, this observable is the *spanning number* n_s, which is the number of loops which connect the top and bottom of a realization. In particular, each loop configuration is realized on a cylinder with circumference $2N$ and lateral height $2N$, which in the Majorana language corresponds to periodic boundary conditions and evolution for $2N$ time steps; the spanning number counts the number of lines that connect the top of the cylinder to the bottom. The spanning number is averaged over loop configurations, weighted by the Boltzmann weights defined above.

The spanning number has an appealing physical interpretation in our free fermion model in terms of entanglement entropy. For specificity we will work with the second Rényi entropy S_2, but we note that for fermionic stabilizer states (like bosonic stabilizer states) all Rényi entropies S_n and the von Neumann entropy are identical. The clearest way to formulate this entropy observable is by bringing in another "ancilla" copy of the many-body Hilbert space, spanned by ancilla Majorana fermions γ'_j, $1 \le j \le 2N$. The initial state is stabilized by the $2N$ bilinears $i\gamma_j\gamma'_j$ which form the generating set; thus the system and the ancilla are maximally entangled with each other. At the final time $2N$, the entanglement entropy between the system and the ancilla is given by $\frac{1}{2}\log 2$ times the number of bilinear generators of the final state that link the system and ancilla. Since this generating set satisfies the clipped gauge condition of Sec. 2.5, this value for the entanglement entropy comes from reasoning similar to that which leads to Eq. 2.17. The base of the logarithm is dependent on the logarithm used to define entropy in this context, and for this chapter it is the natural logarithm. The number of such bilinears is simply the number of worldlines that link the bottom (initial) and top (final) edge of the spacetime i.e., just the spanning number n_s. Thus the final state entropy, averaged over quantum trajectories, is precisely the average spanning number, up to the factor of $\frac{1}{2}\log 2$.

We note that there is another way of viewing this entropy. If we were to focus solely on our system by tracing out the ancillary system, we get a maximally mixed state. Since the free fermion dynamics include measurements, they expose information about the initially mixed state and the system evolves toward a pure state. Then, the entanglement between the system and ancilla is equal to the total (statistical) entropy of the partially mixed state.

Reference [2] shows that the spanning number is an order parameter for the phases that appear in the CPLC. Specifically, there are two primary phases, as shown in the left side of Figure 3.4. The first is the short-loops phase, in which with the spanning number vanishes in the thermodynamic limit where N approaches infinity. Note that this can be further separated into two short-loops phases as described below. The second is a Goldstone phase in which the spanning number scales as $\log N$ in the thermodynamic limit. Note that the name "Goldstone" phase is inherited from the CPLC, in which this phase can be described by the Goldstone phase of a particular nonlinear sigma model. Ref. [2] explores several features of this phase diagram. In particular, it is noted that at $p = 0$ (i.e., the case of measurements only) the CPLC reduces to a model of the bond percolation transition tuned by q. Furthermore, at both $q = 0$ and $q = 1$, it is shown that the field theory describing the CPLC possesses an extra $U(1)$ symmetry which guarantees that the short-loops phase extends all the way to $p = 1$. At values of q different from $q = 0$, $\frac{1}{2}$, and 1, there is a transition from the short-loops to the Goldstone phase at some critical p with $0 < p < 1$. Reference [2] studies this phase transition at $p = \frac{1}{2}$, $q = 0.82$ and extracts a correlation length scaling exponent $\nu = 2.745(19)$.

Further, there is a distinction between the two short-loops phases, which is identified as being a topological distinction. At $q > \frac{1}{2}$ with open boundary conditions, the configurations will tend to have a long macroscopic loop circling the configuration, which is absent when $q < \frac{1}{2}$. This is reminiscent of an edge mode in a topological insulator; thus in the Anderson localization language, these two short-loops phases correspond to trivial and topological insulating phases.

The goal for the remainder of this chapter is to examine the extent to which the CPLC

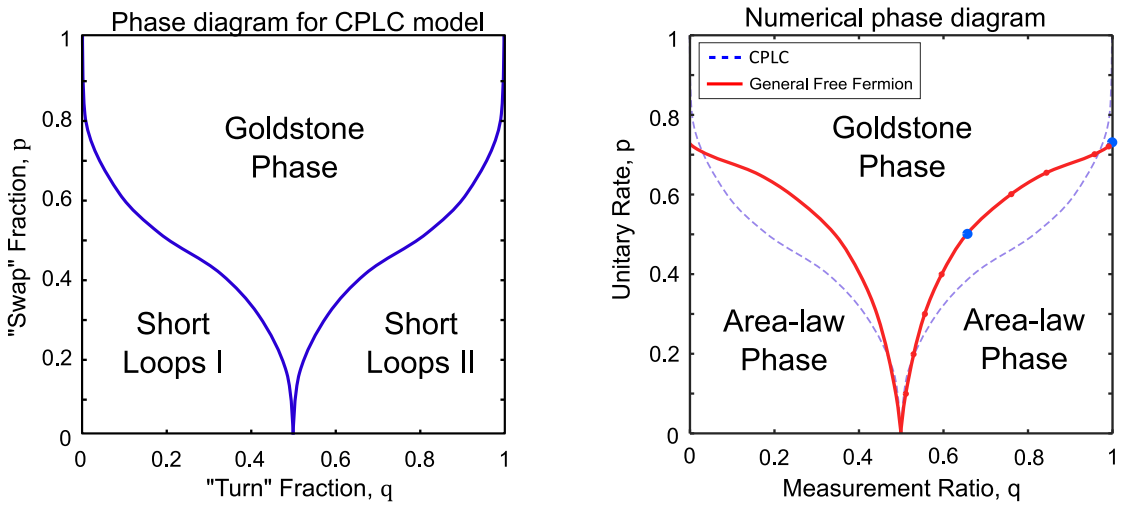

Figure 3.4: (Left) Phase diagram for the CPLC [2]. The difference in Goldstone and Short Loops phases is determined by the behavior of the spanning number, n_s. In the Short Loops phases, the average spanning number $\langle n_s \rangle$ decreases with increasing system size, approaching zero in the thermodynamic limit. In the Goldstone phase, $\langle n_s \rangle$ increases logarithmically with system size. In the more general fermion model, the spanning number generalizes to the second Rényi entropy between the system and ancilla, as described in the text. The difference in the Short Loops I and Short Loops II phases is determined by the existence or absence of a macroscopic loop or edge mode around the configuration; see Fig. 3 of Ref. [2]. (Right) Phase diagram for the more general free fermion model, with CPLC phase diagram for reference. The large blue dots are locations in the phase diagram which are studied in more depth for this chapter. Note the $q \leftrightarrow (1-q)$ symmetry, mentioned in Sec. 3.2. The top line of the diagram at $p = 1$ corresponds an evolution with only unitary gates and no measurements, thus leading to a volume-law phase. The sides of the diagram at $q = 0, 1$ correspond to an evolution with only one type of measurement present, and while the CPLC has no phase transition on these lines, the more general model does.

phase diagram, viewed in terms of the hybrid Majorana dynamics, is robust to more general free fermion dynamics. In order to pursue this, we now introduce the formalism of Gaussian states.

3.3 Generalizing to a Free Fermion Model

To generalize beyond the specific case of the CPLC dual, we will replace the unitary gate $U_{r,r+1}$, which effectively swaps γ_r and γ_{r+1}, with a more general local free fermion unitary gate. In this context, a "free fermion" unitary is one which is generated by fermion bilinear operators i.e., $U = \exp\left(\frac{1}{4}A_{ij}\gamma_i\gamma_j\right)$ with A a real anti-symmetric $2n \times 2n$ matrix. The action of U by conjugation is an orthogonal rotation of the $2n$ Majorana operators:

$$U\gamma_i U^{-1} = \left[\exp(-A)\right]_{ij}\gamma_j$$

In particular, fermionic operators become mapped to a linear combination of fermion operators, instead of a combination of products of operators.

For the measurements, the most general measurements we might want to consider are of the fermion linear optics (FLO) type [45], which can always be thought of as projecting onto eigenstates of some $i\gamma_a\gamma_b$ operator after an appropriate basis transformation. However, for this work we will simply retain the same measurements as in the CPLC dual model introduced above, namely measurements of the operators $i\gamma_r\gamma_{r+1}$.

The generalization we will investigate involves taking the same protocol as Sec. 3.2.1, but replacing the fixed unitary gates $U_{r,r+1}$ with unitary gates which are randomly drawn from the set of all two-Majorana free fermion unitary gates. For the Majorana algebra, all such unitary gates have the action

$$\begin{aligned}\gamma_1 &\to \cos(\alpha)\gamma_1 - \sin(\alpha)\gamma_2, \\ \gamma_2 &\to \sin(\alpha)\gamma_1 + \cos(\alpha)\gamma_2\end{aligned} \tag{3.2}$$

for some angle α. The case of the $U_{r,r+1}$ defined for the CPLC above corresponds to $\alpha = -\frac{\pi}{2}$. In our general model, we will draw α randomly and uniformly from the interval $[0, 2\pi]$.

Because acting with a generic unitary gate of the above form now maps a Majorana operator to a superposition of Majorana operators, we can no longer apply the stabilizer formalism of Section 3.2 to relate the entanglement entropy and the spanning number. Instead, we will perform numerical Monte Carlo studies of the hybrid dynamics. The numerics will start with a maximally mixed state ρ_0 and apply

$$\rho_0 \mapsto \rho = \frac{C\rho_0 C^\dagger}{\mathrm{Tr}(C\rho_0 C^\dagger)} \tag{3.3}$$

where C is a (non-unitary) circuit composed from a product of randomly chosen unitaries and projectors corresponding to a particular quantum trajectory. Specifically, the probability density associated with a particular circuit C is equal to the CPLC Boltzmann weight (a product of powers of p, q, $(1-p)$, and $(1-q)$), multiplied by the uniform probability density associated with the choice of each unitary, multiplied by the Born probability $\mathrm{Tr}\, C\rho_0 C^\dagger$ associated with the measurement outcomes in C. Even though the states appearing in the quantum trajectories are no longer stabilizer states, they still have the property of being "Gaussian", and this allows for efficient numerical simulation. We now review the formalism of these Gaussian states.

3.3.1 Gaussian state formalism

This exposition follows Ref. [45] closely; see Ref. [46] for a more recent introduction. First, we show that the density matrix ρ of a mixed state, when viewed as an operator, has some expansion as a polynomial over the operators γ_j. Every density matrix ρ can always be written as the convex sum of pure state density matrices, $\rho = \sum_j p_j \rho_j$, where $0 < p_j \leq 1$ and $\sum_j p_j = 1$. Each pure state $|\Psi_j\rangle$ corresponding to ρ_j can be written as a superposition of states raised from the vacuum $|0\rangle$ using the creation operators $a_j^\dagger$, and therefore $|\Psi_j\rangle = A_j |0\rangle$ for some A_j which is the linear combination of products of $a_j^\dagger$ i.e., it can be written as a polynomial in $a_j^\dagger$. Then, $\rho_j = |\Psi_j\rangle\langle\Psi_j| = A_j |0\rangle\langle 0| A_j^\dagger$. Noticing that the projector $|0\rangle\langle 0|$ onto the vacuum is given by $|0\rangle\langle 0| = \prod_j a_j a_j^\dagger$, we see that ρ_j has an expansion in terms of a_j and $a_j^\dagger$, and thus so does ρ. Replacing a_j and $a_j^\dagger$ with γ_{2j-1} and γ_{2j} completes the proof.

Given such an expansion, we can form an associated element of a Grassmann algebra by keeping the coefficients and replacing each γ_j with a Grassmann number θ_j. A Grassmann number θ_j is an element of an anticommuting algebra, with $\theta_i\theta_j = -\theta_j\theta_i$ and $(\theta_i)^2 = 0$. These are considered as an independent algebra, and are not to be used alongside the operators of our Hilbert space. ρ is then called Gaussian if the Grassmann algebra element corresponding to its polynomial expansion is of the form

$$\frac{1}{2^N}\exp\left(\frac{i}{2}\theta^T M\theta\right) \tag{3.4}$$

where θ is a $2N$-dimensional column vector of the elements θ_j, and M is a $2N\times 2N$ real anti-symmetric matrix, called the *covariance matrix* in the language of Ref. [46] (or correlation matrix in the language of Ref. [45]) of the state. This covariance matrix describes two-point correlation functions,

$$\frac{i}{2}\mathrm{Tr}(\rho[\gamma_j\gamma_k]) = \begin{cases} \mathrm{Tr}(\rho i\gamma_j\gamma_k) = \langle i\gamma_j\gamma_k\rangle = M_{j,k} & \text{for } j\neq k \\ 0 & \text{for } j = k \end{cases} \tag{3.5}$$

Therefore, Gaussian states have the defining property that all observables can be calculated from no information other than the two-point correlation functions of the state. Each covariance matrix M can be transformed, by an orthogonal rotation, to block diagonal form with N 2×2 blocks on the diagonal. Each block is anti-symmetric, and so determined by a single real number λ_j on the off-diagonal, where $-1\leq\lambda_j\leq 1$ for all j. The $|\lambda_j|$ are called the Williamson eigenvalues of M, and a pure state ρ corresponds to all $|\lambda_j| = 1$.

Let us see how a Gaussian state evolves under our hybrid evolution. First, evolving ρ under free fermion unitary transformations corresponds to a conjugation of M by the rotation in Eq. (3.2), which then rotates the appropriate two-dimensional subspace of θ_j while acting as the identity on the complement. This is a consequence of the fact that $M_{j,k} = \langle i\gamma_j\gamma_k\rangle$, and since the unitary gates act as a rotation of the Majorana fermions, they have a representation as a rotation on the covariance matrix. The result is the covariance matrix of the new state, which remains Gaussian. Now let us consider evolving ρ under a measurement of $i\gamma_j\gamma_{j+1}$

(with post-selection i.e., projecting onto an eigenspace of $i\gamma_j\gamma_{j+1}$ and normalizing). Reference [45] shows that in this case the normalized, post-selected post-measurement state remains Gaussian. Its covariance matrix M', for the measurement outcome $s = \pm 1$, is determined as follows. Let K be the $2N \times 2N$ anti-symmetric matrix whose entries $K_{a,b} = (\delta_{a,j}\delta_{b,j+1} - \delta_{a,j+1}\delta_{b,j})$. In other words, K is zero everywhere except in the 2×2 block corresponding to $(j, j+1)$, in which it is the 2×2 anti-symmetric matrix with the number 1 on the off-diagonal. Let $L = (I - sMK)^{-1}M$. Then we define $M'_{a,b} = L_{a,b}$ if $a, b \notin \{j, j+1\}$, and $M'_{a,b} = sK_{a,b}$ otherwise. The resulting matrix M' has Williamson eigenvalues equal to +1 if M does as well, meaning pure states will evolve into pure states. The probability of the outcome s is $\frac{1}{2}\mathrm{Pf}(M)\,\mathrm{Pf}(sK - M^{-1})$, where $\mathrm{Pf}(\cdot)$ denotes the Pfaffian of an antisymmetric matrix.

We can try to simplify the equation for L using a Taylor expansion in $M_{j,j+1}$ of the form $(1-x)^{-1}$. Since K is only nonzero in the $(j, j+1)$ block, we find that $KMK = -M_{j,j+1}K$. Thus, $(MK)^n = (-M_{j,j+1})^{n-1}MK$, and a Taylor expansion of sMK gives

$$(1 - sMK)^{-1} = 1 + \frac{sMK}{1 + sM_{j,j+1}} \tag{3.6}$$

There are limits on when such a Taylor expansion is justified; however, it can be shown by direct substitution that Eq. (3.6) is indeed the inverse of $(1 - sMK)$. Thus,

$$L = M + \frac{sMKM}{1 + sM_{j,j+1}}$$

Note that performing the evolution takes resources which are polynomial in N, since we follow the covariance matrix rather than the full quantum many body state. This is the advantage of the Gaussian state formalism.

In terms of the Williamson eigenvalues λ_j, $j = 1, \ldots, N$ of M, we can find the eigenvalues of the density matrix ρ, which will be used to calculate the entropy of the state. There exist some linear combinations of Grassmann variables $\xi_j = R_{jk}\theta_k$ in which the correlation matrix M is (block) diagonal, and correspond to the fermionic operators $\gamma'_j = R_{jk}\gamma_k$. Then,

$$\frac{1}{2^N}e^{\frac{i}{2}\theta^\top M\theta} = \frac{1}{2^N}e^{i\sum_j \lambda_j\xi_{2j-1}\xi_{2j}} = \frac{1}{2^N}\prod_{j=1}^{N} e^{i\lambda_j\xi_{2j-1}\xi_{2j}} = \frac{1}{2^N}\prod_{j=1}^{N}(1 + \lambda_j i\xi_{2j-1}\xi_{2j}) \tag{3.7}$$

where we can split the exponential into a product of exponentials because the bilinears $\xi_{2j-1}\xi_{2j}$ mutually commute. Each exponential in the product evaluates to a two term polynomial because $(\xi_{2j-1}\xi_{2j})^2 = 0$. If we write our Hilbert space in terms of the corresponding fermionic operators γ'_j, then we have N fermionic modes, and the operator $i\gamma'_{2j-1}\gamma'_{2j}$ measures the fermion parity $P'_j = \pm 1$ of this mode. Thus[1]

$$\rho = \frac{1}{2^N}\prod_j (1 + \lambda_j i\gamma'_{2j-1}\gamma'_{2j}) = \frac{1}{2^N}\prod_j (1 + \lambda_j P'_j) \tag{3.8}$$

From this, we see that ρ has 2^N eigenvalues given by $2^{-N}\prod_j(1 \pm \lambda_j)$, corresponding to the eigenvectors which are the mutual eigenstates of all $i\gamma'_{2j-1}\gamma'_{2j}$.

Now, we can calculate the entropies. We notice that the density matrix given by Eq. 3.8 is of a simple form. The N modes described by P'_j are independent, and thus we can find the total entropy by adding the entropy of each mode [46]:

$$S_1 = -\mathrm{Tr}(\rho \log \rho) = -\sum_i \left[\frac{1+\lambda_i}{2}\log\left(\frac{1+\lambda_i}{2}\right) + \frac{1-\lambda_i}{2}\log\left(\frac{1-\lambda_i}{2}\right)\right]$$

However, it will be more convenient to work with the second Rényi entropy. The n^{th} Rényi entropy is defined as

$$S_n = \frac{1}{1-n}\log \mathrm{Tr}\rho^n,$$

with the von Neumann entropy being the limit of S_n as $n \to 1$. Note that in this chapter, we take all logarithms to be the natrual logarithm. Again, we can find the total entropy by adding the entropies of each mode, which each have eigenvalues of $\frac{1}{2}(1 \pm \lambda_j)$:

$$\begin{aligned} S_2 = -\log \mathrm{Tr}\rho^2 &= -\sum_{j=1}^{N} \log\left(\frac{1}{4}(1+\lambda_j)^2 + \frac{1}{4}(1-\lambda_j)^2\right) \\ &= -\sum_{j=1}^{N} \log\left(\frac{1}{2}(1+\lambda_j^2)\right) \\ &= \sum_{j=1}^{N} \left(\log 2 - \log(1+\lambda_j^2)\right) \\ &= N\log 2 - \frac{1}{2}\mathrm{Tr}\log(1-M^2). \end{aligned} \tag{3.9}$$

[1]Notice that for pure states, when $\lambda_j = \pm 1$, then ρ is a product of the projectors $\frac{1}{2}(1 + \lambda_j P'_j)$ onto the $P'_j = -\lambda_j$ eigenspace.

In the last step, we used the fact that M^2 has two copies of $-(\lambda_j)^2$ as its eigenvalues. This can be seen by considering the block-diagonal form of M, where the antisymmetric 2×2 matrices square to $-(\lambda_j)^2$ times the 2×2 identity matrix. Therefore, the second Rényi entropy can be extracted from the covariance matrix directly.

3.4 Results

3.4.1 Phase diagram

The above procedures were implemented numerically in MATLAB, where each state is represented as a $2N\times2N$ matrix for various system sizes N between 250 and 2000. The system of $2N$ Majorana fermions evolves under $2N$ time steps before the entropy is calculated via Eq. 3.9. The code was executed on the 'mox' and 'klone' clusters of the University of Washington's high performance computing resource, Hyak. The systems were evolved in parallel using MATLAB's Parallel Computing Toolbox. Most system sizes have on the order of a few thousand realizations or more which are averaged over to calculate the final data.

Our main results are summarized in the phase diagram given on the right side in Fig. 3.4. We find that the two distinct phases persist in the more general free fermion model, though the line separating them has changed. Fig. 3.5 shows the entropy scaling for the point $p = 0.7, q = 0.7$, inside the Goldstone phase, demonstrating that the logarithmic-law scaling persists in the more general model. In Fig. 3.6, we probe the phase transition by varying q for fixed $p = 0.5$, which parallels Fig. 12 in Ref. [2] for the CPLC, and find a continuous phase transition at $q = 0.64(6)$.

One of the distinct differences between the models is the existence of a phase transition on the boundaries of the phase diagram, when $q = 0, 1$. In the CPLC, these values of q introduce an extra symmetry on the model, preventing a phase transition [2]. However, the entropy scaling for the point $p = 0.8$, $q = 0$ is shown in Fig. 3.7, a point which would be in the area-law phase of the CPLC. We instead see a logarithmic-law scaling, demonstrating that it is instead in the Goldstone phase of our model. By probing the entropy as a function

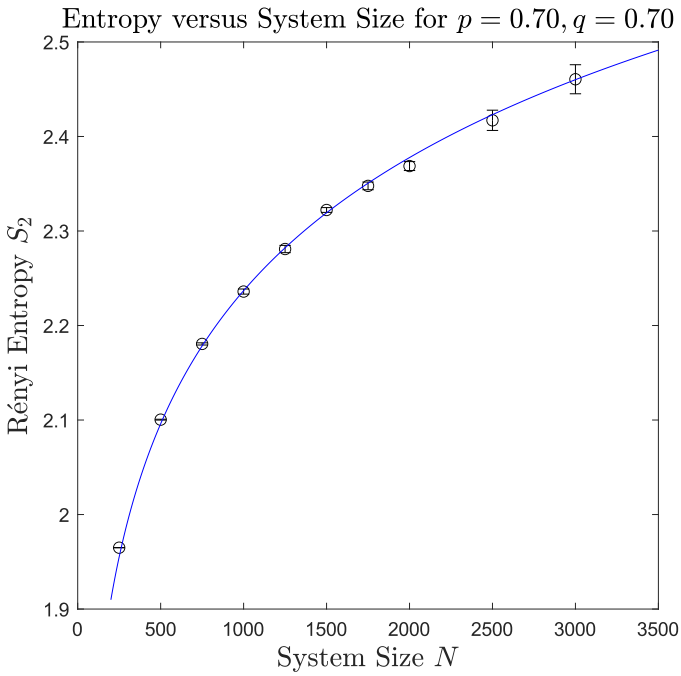

Figure 3.5: Entropy law for a point inside the Goldstone phase in the generalized free fermion model. The blue line is a fit to the logarithm $a\log(bx) + c$. The values obtained were: $a = 0.203$, $b = 0.281$, $c = 1.091$. The 95% confidence bounds on a are $(0.1957, 0.2107)$.

of p for fixed $q = 1$, we find a phase transition at $p = 0.72(2)$, shown in Fig. 3.8.

It is also worth noting that these new phase transitions occur at the most experimentally feasible parts of the phase diagram. At $q = 1$, all measurements in the evolution are of on-site fermion parity, with no multi-site projective measurements. Further, the measurements all mutually commute, giving an entanglement transition that uses commuting projective measurements, which is not seen anywhere else in the phase diagram.

3.4.2 Extracting ν at the generic transition

A finite-size data collapse helps to confirm that this model shows properties of critical phenomena. The underlying idea is that for temperatures close to the critical temperature T_c of

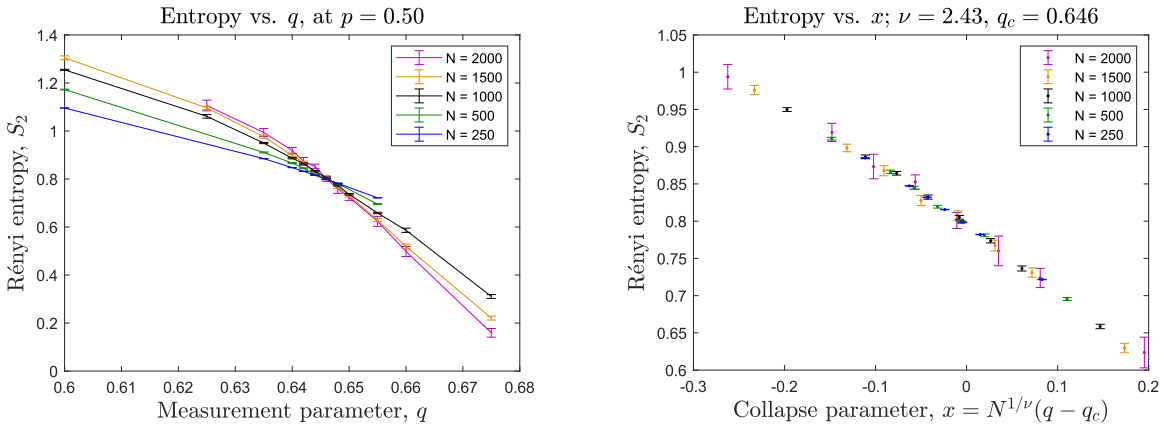

Figure 3.6: Graphs of S for $p = 0.50$, q near 0.64 in the general free fermion model. Most smaller system sizes ($N \leq 1000$) have on the order of $10,000 - 20,000$ realizations which are averaged over, while larger system sizes have on the order of $200 - 2,000$ realizations. The data collapse values for q_c and ν were calculated by fitting the data to a fifth-order polynomial for various values of q_c, ν and finding the values which minimized the residual sum of squares (sum of squares error).

a continuous phase transition, thermodynamic properties should scale as a universal function of L/ξ, where L is the (linear) system size and ξ is the correlation length [31, 47]. For large system size and small reduced temperature $t = (T - T_c)/T_c$, a thermodynamic observable Q should go as

$$Q(L,T) = L^{\kappa/\nu} f(tL^{1/\nu})$$

for some function f. The intuition for the one parameter scaling form $tL^{1/\nu}$ is that as we approach the scale-invariant critical point, a change in length scale can be compensated for by a change in temperature. Here, ν is the correlation length exponent.

In our work, the tuning parameter T is not the temperature but rather p or q, depending on context. Thus, we define

$$x = N^{1/\nu}(T - T_c)$$

and make plots of the entropy S versus this parameter x. By varying the values of ν and

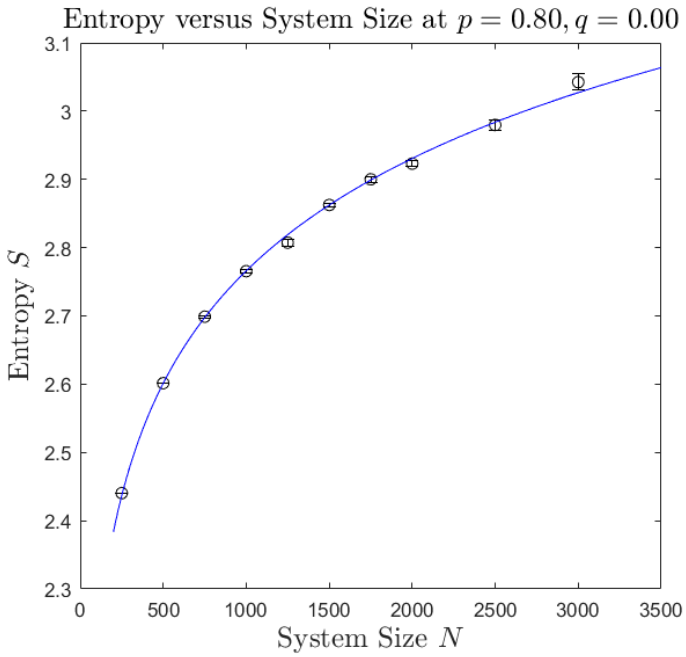

Figure 3.7: Entropy law for a point on the edge of the phase diagram ($q = 0.00$). This point is in the area-law phase (short loops phase) of the CPLC, but inside the Goldstone phase for the general model. The blue line is a fit to the logarithm $a\log(bx) + c$. The values obtained were: $a = 0.238$, $b = 0.646$, $c = 1.228$. The 95% confidence bounds on a are $(0.2282, 0.2473)$.

T_c, we attempt to find the values that give the best collapse of the data points onto a single function of x.

We first study the case $p = 0.50$, with q playing the role of T. The results for this case are shown in Fig. 3.6. We obtain the values for ν and q_c by minimizing the error when fitting the collapsed data to a fifth order polynomial. We obtain values

$$q_c = 0.64(6) \qquad\qquad \nu \approx 2.41(6) \tag{3.10}$$

We note that the value for q_c is smaller than for the $p = 0.5$ transition in the CPLC, which is at $q_{c,CPLC} \approx 0.82$. The value of ν is also smaller, with $\nu_{CPLC} \approx 2.745$ at $p = 0.5$ [2]. However, the uncertainties in ν from numerical errors and possible irrelevant scaling variables leave us

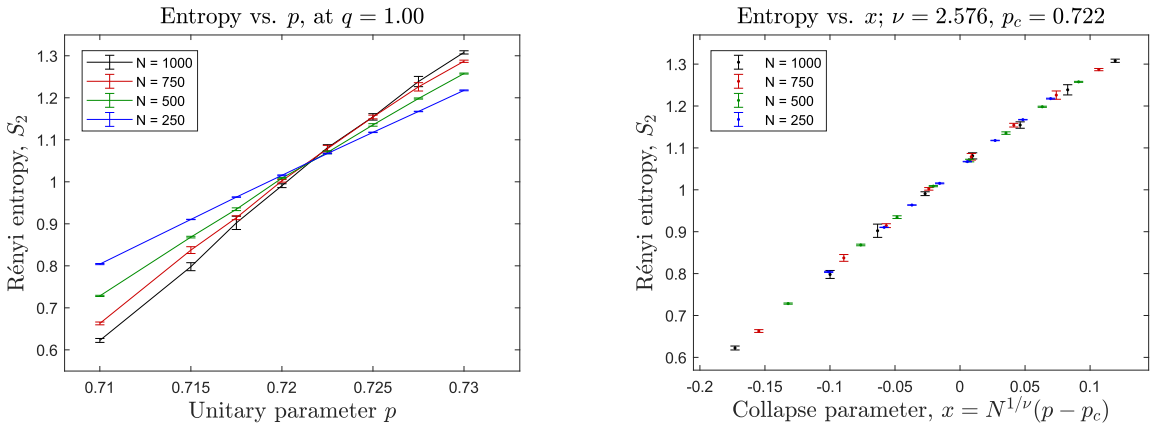

Figure 3.8: Graphs of S for $q = 1.00$, p near 0.72 for the generalized free fermion model. Most smaller system sizes ($N \leq 500$) have on the order of $3,000 - 10,000$ realizations which are averaged over, while larger system sizes have on the order of $100 - 500$ realizations. The data collapse values for p_c and ν were calculated by fitting the data to a fifth-order polynomial for various values of p_c, ν and finding the values which minimized the residual sum of squares (sum of squares error). The data collapse indicates the presence of a continuous phase transition for $q = 1.00$ near $p = 0.72$, a feature of the generalized free fermion model that is not shared with the CPLC.

unable to definitively rule out the possibility that our model is in the same universality class as the CPLC transition.

Further, we find a phase transition at the boundaries of the phase diagram, when $q = 0$ and 1, where none exists in the CPLC. The data for this is shown in Fig. 3.8. Here, we obtain values

$$p_c = 0.72(2) \qquad \nu \approx 2.5(8)$$

This ν is larger than the value found at $p = 0.5$, though still less than what was found for the CPLC. Again, this is consistent with the points being in the same universality class.

3.5 Discussion

In this work we have investigated the purification transition in certain fermionic models of hybrid unitary-measurement dynamics in one dimension. We used an exact duality from the known CPLC classical statistical mechanics model to understand one particular case, and then numerically investigated a particular generalization away from this finely-tuned point. We found that the generalized model retains all of the phases present in the exactly solved model, albeit with shifted phase boundaries. This includes a phase transition at the boundary values $q = 0, 1$ where there were previously no phase transitions. Although we only investigated one specific generalization away from the exactly solvable fixed point, we expect this robustness to persist in general.

One outstanding question that remains is to find a statistical mechanical dual for a general free fermion model in the above class. Quantities such as the second Rényi entropy may be described using a certain replica limit following Section VI of Ref. [48]. Following the strategy which is applied to subsystem entanglement transitions in Ref. [34], one may then hope to interpret such a quantity as the partition function of a statistical mechanics model. One way to do this is to focus on the full replicated system as a single system, where each site hosts a Hilbert space which is the full Hilbert space corresponding to the replicated degrees of freedom at that site. Focusing on the $2n$ Majorana operators at each of these replicated sites, where n is the number of replicas, one can insert a resolution of the identity at each of these replicated site Hilbert spaces, which can be taken as the average over all $\mathrm{SO}(2n)$ rotations of a particular projector. Although it will certainly be difficult to make rigorous statements about the replica limit, one may hope that at least some symmetry based arguments can be made, leveraging the symmetries of the $\mathrm{SO}(2n)$ integrals. For example, one may hope to explain the existence of a phase transition at $q = 0, 1$ in the generalized models, in contrast to the lack of such a transition in the CPLC dual model, by showing that the CPLC dual has an enhanced symmetry at $q = 0, 1$ (see also Ref. [2]).

In addition, the CPLC distinguishes between the two short loop phases, see Fig. 3.4.

The "Short Loops II" phase at $q > \frac{1}{2}$ is distinguished by the existence of a macroscopic loop which circles the configuration when open boundary conditions are used. This is tied to a topological phase in Ref. [2]. The two area-law phases in the generalized model are also tied to the same topological phases, which in the quantum system can be distinguished e.g. by measuring a string order parameter. How to define and numerically measure such an order parameter in an associated statistical mechanics model is a question that we leave for future investigation.

BIBLIOGRAPHY

[1] Yaodong Li, Xiao Chen, and Matthew P. A. Fisher. Measurement-driven entanglement transition in hybrid quantum circuits. *Physical Review B*, 100(13):134306, October 2019.

[2] Adam Nahum, P. Serna, A. M. Somoza, and M. Ortuño. Loop models with crossings. *Physical Review B*, 87(18):184204, May 2013.

[3] Brian Skinner, Jonathan Ruhman, and Adam Nahum. Measurement-Induced Phase Transitions in the Dynamics of Entanglement. *Physical Review X*, 9(3):031009, July 2019.

[4] Michael J. Gullans and David A. Huse. Dynamical Purification Phase Transition Induced by Quantum Measurements. *Physical Review X*, 10(4):041020, October 2020.

[5] Hugo Lóio, Andrea De Luca, Jacopo De Nardis, and Xhek Turkeshi. Purification Timescales in Monitored Fermions. 2023. Publisher: arXiv Version Number: 1.

[6] Crystal Noel, Pradeep Niroula, Daiwei Zhu, Andrew Risinger, Laird Egan, Debopriyo Biswas, Marko Cetina, Alexey V. Gorshkov, Michael J. Gullans, David A. Huse, and Christopher Monroe. Measurement-induced quantum phases realized in a trapped-ion quantum computer. *Nature Physics*, 18(7):760–764, July 2022.

[7] Jin Ming Koh, Shi-Ning Sun, Mario Motta, and Austin J. Minnich. Experimental Realization of a Measurement-Induced Entanglement Phase Transition on a Superconducting Quantum Processor. 2022. Publisher: arXiv Version Number: 2.

[8] Lukasz Fidkowski, Jeongwan Haah, and Matthew B. Hastings. How Dynamical Quantum Memories Forget. *Quantum*, 5:382, January 2021.

[9] Graham Kells, Dganit Meidan, and Alessandro Romito. Topological transitions with continuously monitored free fermions. 2021. Publisher: arXiv Version Number: 3.

[10] DinhDuy Vu, Ali Lavasani, Jong Yeon Lee, and Matthew P. A. Fisher. Measurement-induced Floquet enriched topological order. 2023. Publisher: arXiv Version Number: 1.

[11] Ali Lavasani, Yahya Alavirad, and Maissam Barkeshli. Measurement-induced topological entanglement transitions in symmetric random quantum circuits. *Nature Physics*, 17(3):342–347, March 2021.

[12] Xiao Chen, Yaodong Li, Matthew P. A. Fisher, and Andrew Lucas. Emergent conformal symmetry in nonunitary random dynamics of free fermions. *Physical Review Research*, 2(3):033017, July 2020.

[13] Yaodong Li, Xiao Chen, Andreas W. W. Ludwig, and Matthew P. A. Fisher. Conformal invariance and quantum non-locality in critical hybrid circuits. *Physical Review B*, 104(10):104305, September 2021. arXiv:2003.12721 [cond-mat, physics:quant-ph].

[14] Erik Hostens, Jeroen Dehaene, and Bart De Moor. Stabilizer states and Clifford operations for systems of arbitrary dimensions and modular arithmetic. *Physical Review A*, 71(4):042315, April 2005.

[15] Vlad Gheorghiu. Standard form of qudit stabilizer groups. *Physics Letters A*, 378(5-6):505–509, January 2014.

[16] Joseph Merritt and Lukasz Fidkowski. Entanglement transitions with free fermions. *Physical Review B*, 107(6):064303, February 2023.

[17] D. J. Thouless, M. Kohmoto, M. P. Nightingale, and M. den Nijs. Quantized Hall Conductance in a Two-Dimensional Periodic Potential. *Physical Review Letters*, 49(6):405–408, August 1982.

[18] K. v. Klitzing, G. Dorda, and M. Pepper. New Method for High-Accuracy Determination of the Fine-Structure Constant Based on Quantized Hall Resistance. *Physical Review Letters*, 45(6):494–497, August 1980.

[19] Cui-Zu Chang, Jinsong Zhang, Xiao Feng, Jie Shen, Zuocheng Zhang, Minghua Guo, Kang Li, Yunbo Ou, Pang Wei, Li-Li Wang, Zhong-Qing Ji, Yang Feng, Shuaihua Ji, Xi Chen, Jinfeng Jia, Xi Dai, Zhong Fang, Shou-Cheng Zhang, Ke He, Yayu Wang, Li Lu, Xu-Cun Ma, and Qi-Kun Xue. Experimental Observation of the Quantum Anomalous Hall Effect in a Magnetic Topological Insulator. *Science*, 340(6129):167–170, April 2013.

[20] Xie Chen, Zheng-Cheng Gu, and Xiao-Gang Wen. Local unitary transformation, long-range quantum entanglement, wave function renormalization, and topological order. *Physical Review B*, 82(15):155138, October 2010.

[21] Joshua M Deutsch. Eigenstate thermalization hypothesis. *Reports on Progress in Physics*, 81(8):082001, August 2018.

[22] Dmitry A. Abanin, Ehud Altman, Immanuel Bloch, and Maksym Serbyn. *Colloquium* : Many-body localization, thermalization, and entanglement. *Reviews of Modern Physics*, 91(2):021001, May 2019.

[23] Mark S. Rudner and Netanel H. Lindner. Band structure engineering and non-equilibrium dynamics in Floquet topological insulators. *Nature Reviews Physics*, 2(5):229–244, May 2020.

[24] Yaodong Li, Xiao Chen, and Matthew P. A. Fisher. Quantum Zeno effect and the many-body entanglement transition. *Physical Review B*, 98(20):205136, November 2018.

[25] Yimu Bao, Soonwon Choi, and Ehud Altman. Theory of the phase transition in random unitary circuits with measurements. *Physical Review B*, 101(10):104301, March 2020.

[26] Chao-Ming Jian, Yi-Zhuang You, Romain Vasseur, and Andreas W. W. Ludwig. Measurement-induced criticality in random quantum circuits. *Physical Review B*, 101(10):104302, March 2020.

[27] Matthew P. A. Fisher, Vedika Khemani, Adam Nahum, and Sagar Vijay. Random Quantum Circuits. 2022. Publisher: arXiv Version Number: 1.

[28] Michael Nielsen and Isaac Chuang. *Quantum Computation and Quantum Information: 10th Anniversary Edition*. Cambridge University Press, Cambridge, 2010.

[29] Robert Koenig and John A. Smolin. How to efficiently select an arbitrary Clifford group element. *Journal of Mathematical Physics*, 55(12):122202, December 2014.

[30] Adam Nahum, Jonathan Ruhman, Sagar Vijay, and Jeongwan Haah. Quantum Entanglement Growth under Random Unitary Dynamics. *Physical Review X*, 7(3):031016, July 2017.

[31] Michael E. Fisher and Michael N. Barber. Scaling Theory for Finite-Size Effects in the Critical Region. In *Current Physics–Sources and Comments*, volume 2, pages 8–11. Elsevier, 1988.

[32] Ruihua Fan, Sagar Vijay, Ashvin Vishwanath, and Yi-Zhuang You. Self-organized error correction in random unitary circuits with measurement. *Physical Review B*, 103(17):174309, May 2021.

[33] Shengqi Sang, Yaodong Li, Tianci Zhou, Xiao Chen, Timothy H. Hsieh, and Matthew P.A. Fisher. Entanglement Negativity at Measurement-Induced Criticality. *PRX Quantum*, 2(3):030313, July 2021.

[34] Romain Vasseur, Andrew C. Potter, Yi-Zhuang You, and Andreas W. W. Ludwig. Entanglement transitions from holographic random tensor networks. *Physical Review B*, 100(13):134203, October 2019.

[35] Xiangyu Cao, Antoine Tilloy, and Andrea De Luca. Entanglement in a fermion chain under continuous monitoring. *SciPost Physics*, 7(2):024, August 2019.

[36] Adam Nahum and Brian Skinner. Entanglement and dynamics of diffusion-annihilation processes with Majorana defects. 2019. Publisher: arXiv Version Number: 2.

[37] Shengqi Sang and Timothy H. Hsieh. Measurement-protected quantum phases. *Physical Review Research*, 3(2):023200, June 2021.

[38] Nicolai Lang and Hans Peter Büchler. Entanglement transition in the projective transverse field Ising model. *Physical Review B*, 102(9):094204, September 2020.

[39] Matteo Ippoliti, Michael J. Gullans, Sarang Gopalakrishnan, David A. Huse, and Vedika Khemani. Entanglement Phase Transitions in Measurement-Only Dynamics. *Physical Review X*, 11(1):011030, February 2021.

[40] O. Alberton, M. Buchhold, and S. Diehl. Entanglement Transition in a Monitored Free-Fermion Chain: From Extended Criticality to Area Law. *Physical Review Letters*, 126(17):170602, April 2021.

[41] Qicheng Tang, Xiao Chen, and W. Zhu. Quantum criticality in the nonunitary dynamics of (2 + 1) -dimensional free fermions. *Physical Review B*, 103(17):174303, May 2021.

[42] Xhek Turkeshi, Alberto Biella, Rosario Fazio, Marcello Dalmonte, and Marco Schiró. Measurement-induced entanglement transitions in the quantum Ising chain: From infinite to zero clicks. *Physical Review B*, 103(22):224210, June 2021.

[43] Xhek Turkeshi, Marcello Dalmonte, Rosario Fazio, and Marco Schirò. Entanglement transitions from stochastic resetting of non-Hermitian quasiparticles. *Physical Review B*, 105(24):L241114, June 2022.

[44] M. Żukowski, A. Zeilinger, M. A. Horne, and A. K. Ekert. "Event-ready-detectors" Bell experiment via entanglement swapping. *Physical Review Letters*, 71(26):4287–4290, December 1993.

[45] Sergey Bravyi. Lagrangian representation for fermionic linear optics. *Quantum Information & Computation*, 5(3):216–238, September 2004. arXiv:quant-ph/0404180.

[46] Jacopo Surace and Luca Tagliacozzo. Fermionic Gaussian states: an introduction to numerical approaches. *SciPost Physics Lecture Notes*, page 54, May 2022.

[47] K. S. D. Beach, Ling Wang, and Anders W. Sandvik. Data collapse in the critical region using finite-size scaling with subleading corrections. 2005. Publisher: arXiv Version Number: 1.

[48] Adam Nahum, Sthitadhi Roy, Brian Skinner, and Jonathan Ruhman. Measurement and Entanglement Phase Transitions in All-To-All Quantum Circuits, on Quantum Trees, and in Landau-Ginsburg Theory. *PRX Quantum*, 2(1):010352, March 2021.